INITIAL DESIGN AND ANALYSIS OF INDIGENOUS SYNTHETIC APERTURE RADAR (SAR) DEMONSTRATOR

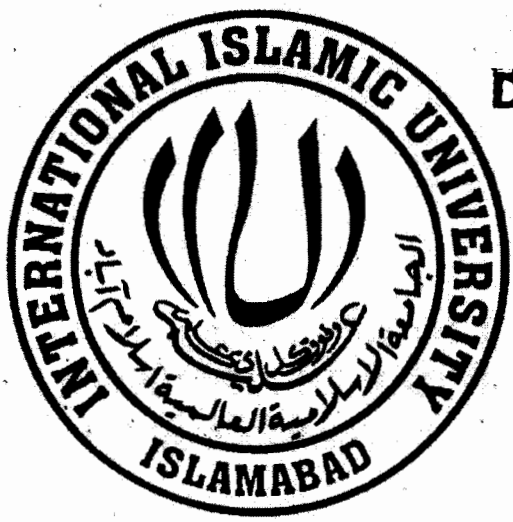

By
Engr. Khan Bahadar Khan
Registration No: 152-FET/MSEE/F08

A thesis submitted in partial fulfillment of the requirements for the Degree of Master of Science in Electronic Engineering with specialization in Communication & Signal Processing at the Faculty of Engineering and Technology, International Islamic University Islamabad.

Supervisor **(December, 2010)**
Dr. Muhammad Usman,
Allied Faculty Member,
International Islamic University Islamabad.

1- Remote sensing

2- Synthetic aperture radar

D.E

2-3-11

Dedicated

To my life partner for her love, support and encouragement during my studies and for bringing so much joy into my life.

In the loving memory of my grandfather, Ghazi Khan Khattak, who impressed on me the value of education and curiosity.

ABSTRACT

A Synthetic Aperture Radar (SAR) is used for all-weather and all-time high resolution aerial and space based imaging of terrain. Being independent of light and weather conditions, SAR imaging has an advantage over optical imaging. Some of the SAR's applications include Surveillance, Targeting, 3D Imaging, Navigation & Guidance, Moving Target Indication and Environmental Monitoring.

During this thesis various small scales SAR programs being developed by various internationals universities and organizations were studied and critically analyzed. Efforts will be made to select suitable design parameters (Operating frequency, Bandwidth, Tx & Rx types and signal processing techniques) based on the technology and capabilities available within Pakistan. This project is aimed at the System-Level Design, Modeling and Simulation of a Synthetic Aperture Radar System and the implementation of its signal processing technique.

The system parameters have been specified in view of all the constraints and practical limitations. The performance metrics of the system such as range resolution and cross-range resolution, etc have been worked out and the system level specification has been selected keeping in view the desired performance. Using MATLAB as major tool, the specified system parameters have been tested for their accuracy and correctness. A simulation of Pulse Doppler radar is performed which includes waveform design, target modeling, LFM pulse compression, side lobe control and threshold detection. A SAR image formation algorithm (Doppler Beam Sharpening) has been implemented in MATLAB and compared with available data on internet.

ACKNOWLEDGEMENTS

I would like to express my sincere gratitude to God Almighty, the most Merciful and the most Gracious for the blessing bestowed upon and the courage, strength and determination which He has given to me for making this dissertation possible.

I am especially very thankful to my supervisor **Dr. Muhammad Usman** (Faculty member, IIUI), for all his guidance, support and numerous technical inputs in shaping this project from its embryonic stage to its final stage. I also want to acknowledge **Dr. Arbab Ali Khan** (FET Dy.Dean, IIUI) for his assistance and sincere suggestions. I wish to express my acknowledgments to **Dr. Ihsan-ul-haq** (Faculty member, IIUI) for his superb coordination during the project.

In addition, I wish to thank all the graduates at FET specially **Abdur Rehman** (Manager-Technical, NESCOM) and **Tahir Saleem Khattak** (PhD Scholar) for all their help and assistance in writing up this dissertation.

Finally, many thanks to my parents, to my brothers & sisters and to my all friends for their love, support and encouragement during my studies. Especially I am very thankful to my life partner for her financial support throughout my graduate studies.

Engr.Khan Bahadar Khan

Table of Contents

LIST OF TABLES

LIST OF FIGURES

LIST OF ABBREVIATIONS

AESA	Active Electronically Scanned Array
BYU	Brigham Young University
COTS	Commercial-Off-The-Shelf
CCD	Coherent Change Detection
CP-SAR	Circularly Polarized Synthetic Aperture Radar
DARO	Defense Airborne Reconnaissance Office
DARPA	Defense Advanced Research Projects Agency
DBS	Doppler Beam Sharpening
ERS	European Remote Sensing satellite
ECR	Earth Centered Rotating (Coordinate System)
GA	General Atomics
IMU	Inertial Motion sensing Unit
LIMEX	Labrador Ice Margin Experiment
LRU	Line Replaceable Unit
LFM-CW	Linear frequency modulated continuous wave signal
NOAA	National Oceanic and Atmospheric Administration
PRF	Pulse Repetition Frequency
SIR- C/X-SAR	Shuttle Imaging Radar-C/X-band Synthetic Aperture Radar
SAR	Synthetic Aperture Radar
SLAR	Side Looking Airborne Radar
SRTM	Shuttle Radar Topography Mission
SELEX	Sensors and Airborne Systems, a Finmeccanica Company
SAR/GMTI	Synthetic Aperture Radar/Ground Moving Target indication
TNO-FEL	Physics and Electronics Laboratory, Netherland

CHAPTER 1 INTRODUCTION

1.1 Objective of the Thesis

There are two major objectives of the thesis. First one is the preparation of feasibility report for designing and development of indigenous Synthetic Aperture Radar (SAR) demonstrator. During this project various small scales SAR programs being developed by various internationals universities and organizations are studied and critically analyzed. Efforts will be made to select suitable design parameters (Operating frequency and Bandwidth, Tx and Rx types and signal processing techniques) based on the technologies capabilities available within Pakistan.

The second objective is the image processing method based on time domain correlation will be used to simulate the SAR system based on the parameters selected above. The second part is being software design which is covered in Simulation & Results part of the thesis, includes the development of signal processing techniques to analyze and display the data and formulate an image.

1.2 Organization of the Thesis

The thesis consists of eight chapters. The brief descriptions of these remaining chapters are given below.

In order to understand the phenomena of Synthetic Aperture Radar (SAR), its early development and fundamentals of SAR Sensors are included in Chapter 2. It starts with an introduction of SAR, which gives a view of how it works and how it acquired image. Brief description of early SAR developments is also discussed. Early

developed spaceborne and airborne sensors by different organization and universities are also included.

Chapter 3 starts with a short overview and operation modes of SAR. It provides a detailed description of SAR geometry. SAR signal in its range and cross-range direction and its data acquisition is also discussed in this chapter.

Chapter 4 consists of SAR design parameters considerations. Various small scales SAR programs being developed by various internationals universities and organizations studied and critically analyzed and hardware design parameters for our proposed SAR system is also presented.

Chapter 5 is reserved to discuss the research work being carried out in the exciting field of development of SAR by different organizations and universities. Early airborne SAR systems parameters comparison is also part of the chapter.

Chapter 6 provides overview of all the processing techniques used in Simulation of SAR image.

Chapter 7 presents the simulation work performed in Matlab/Simulink and the results obtained. Comparison of simple and LFM pulse is shown. Range and cross-range resolution results are obtained by applying matched filtering and DBS algorithm. The results are compared, discussed and any shortcomings are analyzed.

Chapter 8 provides the conclusions and recommendations for future research.

the radar approaches a target; decrease as it moves away). Comparing the Doppler-shifted frequencies to a reference frequency allows many returned signals to be "focused" on a single point, effectively increasing the length of the antenna that is imaging that particular point. This focusing operation, commonly known as SAR processing, is now done digitally on fast computer systems. The trick in SAR processing is to correctly match the variation in Doppler frequency for each point in the image: this requires very precise knowledge of the relative motion between the platform and the imaged objects (which is the cause of the Doppler variation in the first place).

Synthetic aperture radar is now a mature technique used to generate radar images in which fine detail can be resolved. SARs provide unique capabilities as an imaging tool. As they can image at any time of day or night, regardless of sun illumination. SARs can also "see" through cloudy and dusty conditions that visible and infrared instruments cannot because of their longer wavelength [2]. SAR can also gather data in conditions where optical sensors would become useless, i.e. it can provide excellent images of what the radar detected even in fog, clouds or darkness. SAR data is used to study agriculture, ecology, geology, oceanography, and hydrology as well as shipping in ice-covered seas, oil exploration, ocean pollution monitoring, and ocean research and can be utilized for many more applications [2].

SAR produces a two-dimensional image. One dimension is called range (or cross track) and is a measure of the "line-of-sight" distance from the radar to the target. Range is determined by precisely measuring the time from transmission of a pulse to receiving the reflection from a target. The other dimension is called azimuth (or along track) and is perpendicular to range. To obtain fine azimuth resolution, a

physically large antenna is needed to focus the transmitted and received energy into a sharp beam. Large apertures are required in order to obtain fine imaging resolution (antenna lengths of several hundred meters are often required). The distance the aircraft or moving platform covers in synthesizing the antenna is known as the synthetic aperture [3].

2.2 History of SAR

While investigating methods of SAR imaging, the history of SAR and radar is important. SAR designs and related applications have grown exponentially since the 1950s when Dennis Gabor [4], the engineer at British Thomson-Houston invented holography in 1947. He laid the groundwork for SAR with the principles of wavefront reconstruction. Carl Wiley [2] of Goodyear Aerospace discovered post processing of the Doppler shift information. This provided the ability to obtain finer resolution in the direction of the travel of the beam. Using the Doppler shift post processing and wavefront reconstruction theory, in 1951 Wiley developed the process known as SAR imaging. By which two-dimensional images of targets and the earth's surface could be constructed using radar [4-6]. Table 2.1 provides a brief overview of SAR development [7].

Industrial and military developments continued at Goodyear, Hughes, and Westinghouse, using airborne platforms. The Environmental Research Institute of Michigan (ERIM), University of Michigan, Sandia Laboratories, Jet propulsion Laboratory (JPL) and other also began to explore this new technology. In 1974, engineers at JPL formed an alliance with a group of international ocean scientists led by the National Oceanic and Atmospheric Administration (NOAA) to determine if an ocean application satellite featuring a space-based SAR could be achieved.

DATE	DEVELOPMENT
1951	Carl Wiley of Goodyear introduces the Doppler beam-sharpening concept.
1952	University of Illinois demonstrates the beam-sharpening concept.
1957	University of Michigan produces the first SAR imagery using an optical correlator.
1964	Analog electronic SAR correlation demonstrated in non-real time (University of Michigan).
1969	Digital electronic SAR correlation demonstrated in non-real time (Hughes, Goodyear, and Westinghouse).
1972	Real-time digital SAR demonstrated with motion compensation (for aircraft systems).
1978	First Space-borne SAR NASA/JPL SEASAT satellite. Analog downlink; optical and non-real-time digital processing.
1981	Shuttle imaging Radar series starts –SIR-A. Non-real time optical processing on ground.
1984	SIR-B. Digital downlink; non-real-time optical processing on ground.
1986	Space-borne SAR Real-time processing demonstration using JPL Advanced Digital SAR processor (ADSP).
1987	Soviet 1870 SAR is placed in earth orbit.
1990	Magellan SAR images Venus.
1990	Evolution of SAR begins in space; Soviet ALMAZ (1991), European ERS-1 (1991), Japanese JERS-1 (1992), SIR-C (1994), ERS-2 (1995), Canadian RADARSAT-1 (1995), SRTM(2000), ENVISAT (2002).

Table 2.1: Highlights of SAR History

Up until this time, the major emphasis of space-based remote sensing had been on land applications using visible and infrared sensors. SEASAT was launched in June 1978, to collect information on sea temperature, sea ice, wind speed and direction, and wave heights [8]. SEASAT first demonstrated the beneficial use of synthetic aperture radar. SEASAT was followed by Shuttle Imaging Radar-A (SIR-A) and Shuttle Imaging Radar-B (SIR-B) launched in 1981 and 1984, respectively [9, 10].

Both the SIR-A and SIR-B radars were variations on the SEASAT radar operating at L-Band and HH (horizontal transmit, horizontal receive) polarization.

The 1980s saw only Space Shuttle based, SEASAT derivative, spaceborne SAR activity, with the exception of the Soviet 1870 SAR (not widely distributed). A significant expansion of SAR missions with the launch of five earths's oriented SAR satellites along with two more Shuttle Imaging Radar missions were witnessed in 1990s. Magellan SAR was used to map Venus. The satellite systems ALMAZ [11], European Remote Sensing (ERS) [12], the Japanese Earth Resources Satellite (JERS)-1 [13], ERS-2 [14] and RADARSAT-1 [11], each operated at a single frequency and single polarization, like SEASAT. ALMAZ and RADARSAT-1 had the additional ability to operate at various incident angles. RADARSAT-1 also has a frequently used ScanSAR mode, where the coverage swath extends up to 500 km.

Shuttle Imaging Radar-C/X-band SAR (SIR-C/XSAR) flown in April and October 1994, one of the most advanced SAR system, was a joint NASA/German Space Agency/Italian Space Agency mission [15]. The system could be operated simultaneously at three frequencies (L, C, and X) with the C-and L-band having the ability to alternately transmit and receive at both horizontal and vertical polarization [16]. In 2002 for the Shuttle Radar Topography Mission (SRTM), the C-and X-band portions of the SIR-C radar were again flown. Table 2.2 provides a list of the earth orbital SAR missions and their characteristics [17].

Future SAR missions are expected to provide enhanced capabilities, where the radar can be operated in several collection modes. ESA's ENVISAT, the follow-on to ERS-1 and ERS-2 was placed in orbit in March 2002. The upcoming RADARSAT-2

and Japan's ALOS Phased Array L-band SAR (PALSAR) instruments will both have fully polarimetric and Scan SAR operating modes.

Satellite	Country	Year	Band	Freq. (GHz)	Wavelength (cm)	Incident Angle (degree)	Pulse Bandwidth (MHz)/Range Resolution(m)	Azimuth Resolution(m)/(Looks)
SEASAT	USA	1978	L-band	1.275	23.5	23	19/(7.9)	6/(1)
SIR-A	USA	1981	L-band	1.275	23.5	50	6/(24.9)	6.5/(1)
SIR-B	USA	1984	L-band	1.275	23.5	15-65	12/(12.5)	6/(1)
ERS-1/2	Europe	1991/5	C-band	5.25	5.7	23	15.5/(9.7)	25/(3)
ALMAZ	USSR	1991	S-band	3.0	10	30-60	-/15	15/(2)
JERS-1	Japan	1992	L-band	1.275	23.5	39	15/(10)	30/(4)
SIR-C/ X-SAR	USA Germany	1994	L-band C-band X-band	1.25 5.3 9.6	23.5 5.7 3	15-55 54	 10/(15) 20/(7.5)	7.5/(1) 6/(1)
RADARSAT-1	Canada	1995	C-band	5.3	5.7	20-50	11.6/(12.9) 17.3/(8.6) 30/(5)	28/(4) 50/(2-4) 100/(4-8))
SRTM	USA Germany	2000	C-band X-band	5.25 9.6	5.7 3	54 54	20/(7.5) 8/(18.7)	15/(1) 8-12/(1)
ENVISAT	Europe	2002	C-band	5.25	5.7	15-45	9/(16.6)	6/(1) 150/(12 1000/(18-21)

Table 2.2: Characteristics of earth orbital SAR systems

2.3 Spaceborne SAR Sensors

The main SAR sensors for which the algorithms have been developed are introduced below. Characteristics of SAR sensors are listed in Table 2.2.

2.3.1 SEASAT

SEASAT was the first civilian spaceborne SAR launched in 1978 and drew the attention of the remote sensing community to the benefits of SAR. It operates at L-band (1.27 GHz) with an incidence angle of 23 degree. The large range cell migration of the received data was a significant factor in processor design. It inspired a significant design effort in digital processing and many processors in use today trace their genealogy back to SEASAT.

2.3.2 Magellan

The NASA/JPL Magellan spacecraft was launched on May 4, 1989 and arrived at Venus on August 10, 1990. The spacecraft was based on a Voyager bus and utilized a 4-m circular dish for the SAR antenna. The radar frequency was 2.4 GHz (S-Band). In the two-year SAR mapping mission, over 98% of the surface was mapped with a resolution of 100m.

2.3.3 ALMAZ

The Russian SAR satellite, ALMAZ, was launched in 1991, but it did not have much exposure in the western remote sensing community. Its main unique feature was its operation at S-band (3.0 GHz).

2.3.4 SIR-C/X-SAR

SIR-C was the third of a series of NASA SAR systems to fly on the space shuttle. Its main features were operation at three frequencies, L-, C- and X-band and the use of quad-polarization on L- and C-band. The X-band SAR system was provided by Germany and Italy. The multiple channels spawned a rich set of applications research projects, which have helped define the requirement for subsequent SAR systems.

2.3.5 ERS-1/2

The European Remote Sensing satellite (ERS-1) was launched in 1991 represented a major effort in global cooperation. Twelve European nations and Canada combined to build a mutli-instrument microwave satellite [4]. The SAR operated at C-band and other instruments included an altimeter, radiometer and

scatterometer. The SAR specifications were similar to SEASAT with the exception of the wavelength.

ERS-2 was launched in 1995 with the same specifications as ERS-1. Its main unique feature was its operation in tandem with ERS-1, which opened up the field of repeat-pass satellite SAR interferometry. With a one-day interval between observations, images that were taken from almost the same vantage point could be used to measure terrain height and to detect changes in surface features.

2.3.6 J-ERS

The Japanese Earth Remote Sensing satellite (J-ERS) was launched in 1992. It had similar specifications to SEASAT but had a larger incidence angle, optimized for geological applications.

2.3.7 RADARSAT-1

The RADARSAT-1 satellite was launched by the Canadian Space Agency in 1995. It operates at C-band and its main use is the daily mapping of Article ice. Its main innovation is a scanning mode of operation called ScanSAR, whereby very wide swaths are imaged by scanning the radar beam to different elevation angles within the synthetic aperture time. Swath widths of 300 km are obtained with four scanned beams.

2.3.8 SRTM

The Shuttle Radar Topography Mission in February 2000 represented the third flight of SIR-C and X-SAR.

2.3.9 ENVISAT/ASAR

The Third European satellite SAR system was launched in February 2002 and is providing good quality data. It was build upon ERS-1 and ERS-2 technology by providing two polarization plus wide swath and ScanSAR modes.

2.4 Different SAR Programs

There are a large numbers of SAR sensors designed by various universities and organizations. In this section we will discuss some of them.

2.4.1 Lynx by Sandia National Laboratories

Lynx was high resolution Synthetic Aperture Radar (SAR) which was designed and built by Sandia National Laboratories and incorporates General Atomics (GA). The purpose of designing lynx SAR was to address a wide variety of manned and unmanned missions. Lynx may be operated on different platforms manufactured by General Atomics (GA) which includes the Predator, I-GNAT or Prowler II platforms. It may also be operated on manned platforms. Lynx was developed entirely on GA corporate funds. GA is presently beginning the manufacture of Lynx and intends to sell Lynx units and Lynx services to military and commercial customers. Lynx is multimode radar. Spotlight mode and stripmap or search mode are its two SAR modes. Ground moving target indicator (GMTI) is its additional operating mode. Coherent change detection (CCD) mode of Lynx indicates minute changes in two SAR images taken at different times. CCD may perform with either spotlight or stripmap images. A uniquely flexible user interface is also feature of Lynx. Due to this feature a view manager allows Lynx to pan and zoom like a video camera. A conventional waterfall display for stripmap display also features of Lynx. Lynx operates at Ku band and is capable of 0.1 m resolution in spotlight mode and 0.3 m

resolution in stripmap mode. It has a slant range of 30 km and weights less than 125lb (56.69 kg) [18].

2.4.2 MiniSAR

The TNO Physics and Electronics Laboratory have been involved for many years in the research of Radar Remote Sensing. Phased Array Universal SAR (PHARUS) was developed in 1988 started as a logical next step after years of experience with real-aperture Side Looking Airborne Radar (SLAR). Active phased array technology was used in PHARUS which is polarimetric SAR system [19]. The high exploitation cost of the system and limited availability are the shortcomings. To address this need, TNO is developing a miniature, lightweight, low-cost, scalable SAR/MTI system called 'MiniSAR'. The system will be based on commercial-off-the-shelf (COTS) components as much as possible. Implying electronic beam-steering capability, the antenna will be designed with active phased array technology. Foreseen major applications for the system are: topographic mapping and map updating, monitoring of infrastructure and surveillance, e.g. oil and gas pipelines and local deformation and subsidence monitoring. In addition for a medium-altitude Unmanned Aerial Vehicle (UAV), the system will be deployed as a SAR. In a low-cost motorglider platform the prototype system will be integrated initially. In the pod of the Stemme motorglider the prototype system will be integrated. For this, the weight should be constrained to less than 50 kg. Its operating modes are stripmap, spotlight, forward-and side-locking three-channel ground moving target indicator and interferometric SAR [19].

2.4.3 PicoSAR

SELEX Sensors and Airborne Systems (S&AS) UK produced the PicoSAR Active Electronically Scanned Array (AESA) provides an unrivalled all weather capability for unmanned Aerial Vehicles (UAV), fixed wing and helicopter platforms. Using AESA technology in a small and compact configuration is the key to picoSAR. The picoSAR radar is more reliable than conventional radar systems using many low powers, solid state Transmit/Receive Modules (TRM) within its array. PicoSAR's have ability to steer the radar beam electronically for the most compact installation. It can be mounted directly onto the platforms or for an even greater field of view, it can be moving pedestal mounted. PicoSAR consists of a single small Line Replaceable Unit (LRU). If the ease of installation issues is required the LRU can be reconfigured by splitting the unit into two parts, one is antenna/IMU and second is supporting hardware (processor, GPS card, etc.). PicoSAR delivers a high resolution Synthetic Aperture Radar (SAR) imaging and Ground Moving Target indication (GMTI) capability that permits new and existing platforms to easily obtain a true all-weather ground mapping and surveillance capability. PicoSAR installation in parallel with electro optical / infrared sensors even on the platforms with heavily constrained payload capabilities is possible due to its compact size, low weight and low power consumption [20].

2.4.4 MicroSAR by Brigham Young University (BYU)

A new low-cost Micro Synthetic Aperture Radar (μSAR) was developed by BYU in 2002. The simple design based on a linear frequency modulated continuous wave signal (LFM-CW). It has compact size and less consumption of power as compared to a conventional pulsed SAR system. This enables the BYU μSAR to fly on a small unmanned aerial vehicle (UAV). Its low cost of operation

extended its use into new areas. μSAR system consists of a stack of custom microstrip circuit boards in order to minimize size, weight and cost of the BYU μSAR. By using no enclosure the weight of the overall system is reduced further. Its weight is less than 2 kg in all, including antennas and cabling. Transmitter, Receiver, power, digital and A/D systems are five subsystem of the μSAR system architecture. Each subsystem is built upon its own customs board or shared between boards. Coaxial cables and wires are used for the interconnection of subsystems. The μSAR is designed for "turn-on and forget" operation. The system collects data continuously for up to an hour once powered up. For post-flight analysis, the data is stored on board [21].

CHAPTER 3 THEORY OF SYNTHETIC APERTURE RADAR

3.1 SAR system Overview

This section presents short overview of SAR system and its working modes. Presently Synthetic Aperture Radar has attained a very great importance due to its ability of working day-night and having capability of working in all weather conditions and also of its increased resolution. Typical SAR system consist of radar set which is mounted on an aircraft, which is transmitting pulsed waveforms and receiving backscattered energy while flying around the scene of interest. In general, a target present at the scene of interest reflects the electromagnetic energy which is received by the antenna mounted on the aircraft. For the formation of a SAR image these received energy or backscatters signals from the targets are processed. The most commonly used signal for illuminating the ground patch is the linear FM chirp signal given by,

$$s(t) = \begin{cases} e^{j(\omega_{0t} + \alpha 0 t^2)}, & |t| \leq \frac{T_p}{2} \\ 0, & \text{otherwise} \end{cases} \qquad (3.1)$$

where ω_0 is the center carrier frequency, $2\alpha_0$ is the chirp rate and T_p is the total pulse duration. The distance of a target can be measured by the delay between transmitted and received signals. A scene perpendicular to aircraft flight path is illuminated by the radar, the direction perpendicular to flight path is called range or downrange direction and the one parallel to it is called the cross range direction.

3.1.1 SAR Operation Modes

A SAR can be operated in a number of different ways, sometimes with different systems and sometimes as different modes within a single system. Six different modes of operations are discussed in following subsections.

3.1.1.1 Stripmap SAR

In Stripmap mode antenna is pointed at a fixed angle during the data collection along the flight path as shown in Figure 3.1. It means that the antenna scans over a particular area which is parallel to the flight path. The antenna can be squinted forward, backward or just perpendicular relative the flight path. In this way a target is illuminated for a limited amount of time.

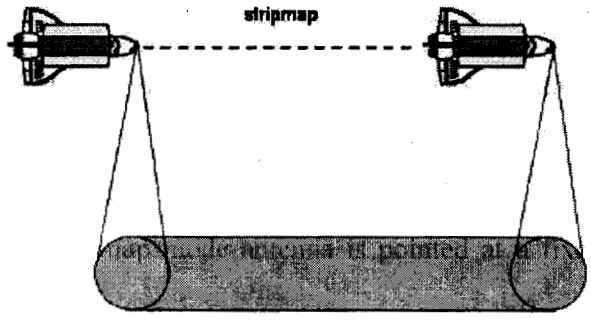

Figure 3.1: Stripmap Mode of SAR

3.1.1.2 Spotlight SAR

In Spotlight mode antenna is steered mechanically or eclectically to illuminate the particular area during the entire flight path as shown in the Figure 3.2. A very long synthetic antenna is created by this mode. The spotlight mode differs from strimap mode in the following way:

1. Spotlight mode illuminates the same area during the entire flight path which is not the case for stripmap. In spotlight mode the length of synthetic antenna is much longer than stripmap mode.

2. The resolution of spotlight is better then stripmap.
3. The angle of illumination for the stripmap mode is fixed and given by squint angle whiles spotlight mode uses much wider angular variation to illuminate the target.

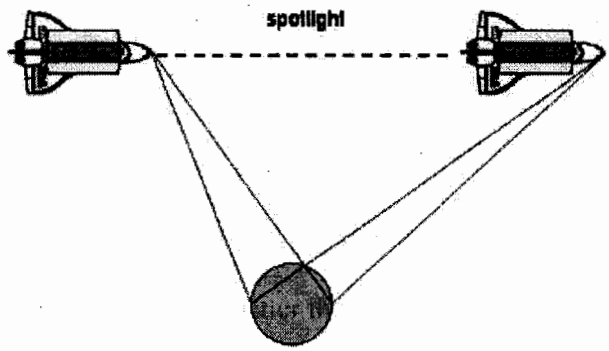

Figure 3.2: Spotlight Mode of SAR

3.1.1.3. ScanSAR

In scan mode the antenna is steered to illuminate a strip of terrain at any angle relative the flight path as shown in Figure 3.3. This mode is a variation of stripmap SAR, whereby the antenna scans range several times during a synthetic aperture. This way a much wider swath is obtained, but the azimuth resolution is degraded. The best azimuth resolution that can be obtained is that of the stripmap mode multiplied by the numbers of swaths scanned [4]. The removal of the antenna positioning direction is the difference between scan mode and stripmap mode.

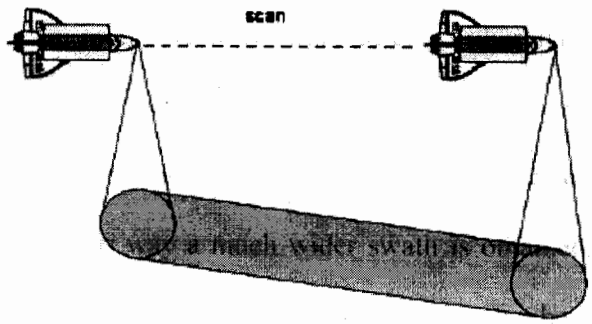

Figure 3.3: ScanSAR Mode of SAR

3.1.1.4. Inverse SAR (Ground Based SAR)

So far, it has been assumed that the target is stationary and the SAR system is moving. However, SAR also works if the target is moving and the radar system is stationary. This reversal of role leads to the term "Inverse SAR" [4]. The working of inverse mode is similar to spotlight mode as shown in Figure 3.4. Instead movement of the antenna, it uses a stationary antenna and a moving target.

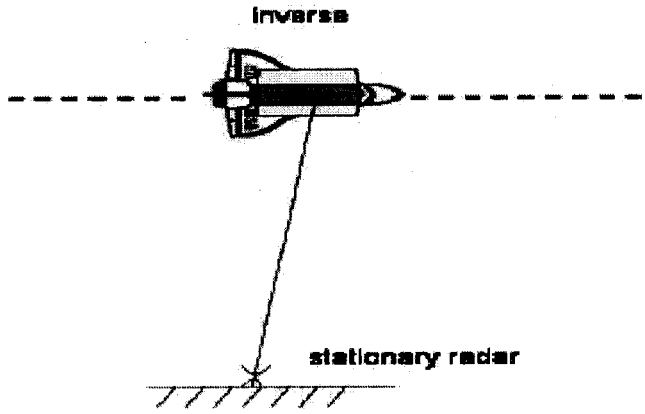

Figure 3.4: Inverse Mode of SAR

3.1.1.5. Bistatic SAR

This is a mode of SAR operation in which the receiver and the transmitter are at different locations. In remote sensing SARs, the receiver is usually at approximately the same location as the transmitter, which is referred to as monostatic.

3.1.1.6. Interferometric SAR (InSAR)

This is a mode of SAR operation in which post-processing is used to extract terrain height or displacement from the complex images. Two complex SAR images acquired at the same spatial position (differential InSAR) or slightly different positions (terrain height InSAR) over the same area are conjugate multiplied. The result is an interferogram with contours of equal displacement or elevation.

3.1.2 Synthetic Aperture in SAR Context

The main purpose of this section is to explain the term "synthetic aperture" in SAR context. This gives another derivation of the azimuth resolution. The azimuth resolution before processing of conventional radar or a SAR is given by the azimuth beamwidth. Radar wavelength λ and the antenna length or aperture is used to determine the beamwidth. For a given radar system both these parameters are fixed. To reduce the effective beamwidth would be desirable to improve the resolution. Similar to synthesizing a narrow pulse in range, the trick is to use signal processing to synthesize a narrow beamwidth in azimuth. Since the beamwidth is inversely proportional to the antenna aperture. So synthesizing a narrow beamwidh is equivalent to synthesizing a large aperture. In practice, in the airborne case the synthesized aperture can be several hundred meters long and several thousand meters long in the spaceborne case. Whereas the antenna's real aperture is only on the order of 1 to 15 m in length.

3.1.3 General Structure of SAR System

General structure of SAR system is shown in Figure 3.5. A pulse is created by pulse generation unit with a bandwidth according to the aspired range resolution. Pulses are amplified by sender and repeater is used to transfer these pulses to the antenna. The receiver gets the antenna output signal amplifies them to an appropriate level and applies a bandpass filter. The calculation of SAR image by SAR processor started after demodulation and analog to digital conversion of the signals. Motion measurement sensor is used to provide additional motion information. To arrange Operation sequence and particularly the time schedule is done by the radar control unit.

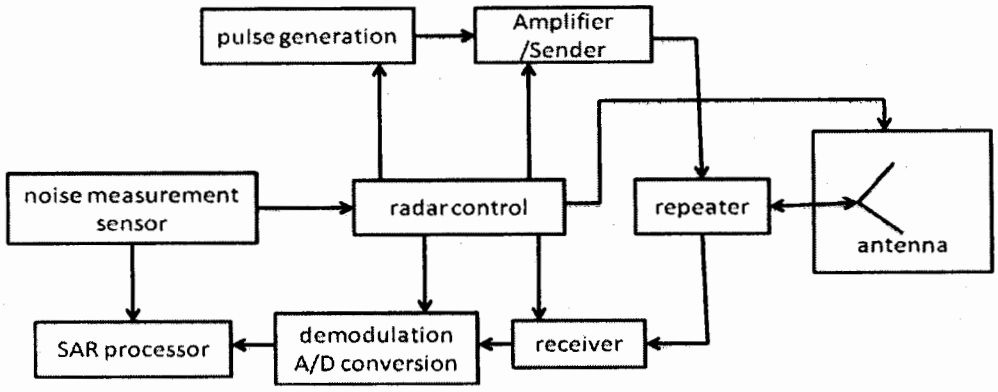

Figure 3.5: General structure of SAR system

3.2 SAR Geometry

The purpose of this section is to clarify SAR data acquisition geometry and geometry related terms.

3.2.1 Definition of Terms

Figure 3.6 shows a simple geometric model of the radar data acquisition [22] and the beam footprint on the Earth's surface. Radar systems can be monostatic, bistatic, or multistatic, depending upon the location of the receiver in relation to the transmitter. The terms used to explain SAR geometry are defined as follows [4].

Target: This is supposed position on the Earth's surface that is imaged by the SAR system. To build up the SAR equations, a single representative point on the ground is considered. This point is called a "point scatterer" or "target point" or simply "scatterer" or "target".

Beam footprint: The radar antenna projects a beam onto an area of the ground referred to as the beam "footprint" during the transmission of a particular pulse. The

position and shape of the footprint depend on the antenna beam pattern and the sensor geometry. This footprint is said to be "illuminated" by the radar beam.

Nadir: The nadir is the point on the Earth's surface directly below the sensor, so that the "normal" to the Earth's surface at the nadir passes through the sensor.

Radar Track: As the nadir point moves along the Earth's surface, it traces out the radar track.

Velocities: There are two system velocities to consider [4]:

- Platform Velocity: This is the velocity, denoted by Vs, of the platform along the flight path.
- Beam Velocity: This the velocity, denoted by Vg, with which the zero Doppler line sweeps along the ground. It is different from Vs when antenna scans along with the direction of Vs.

Azimuth: Azimuth is a direction aligned with the relative platform velocity vector. It can be considered as a vector parallel to the net sensor motion, as in Figure 3.6 [4].

Zero Doppler planes: The sensor in this plane is at right angle to the platform velocity vector (in the ECR coordinates). It is approximately perpendicular to the azimuth axis, where the approximation comes from the fact that the platform may be climbing or descending. The intersection of this plane with the ground is called the zero Doppler line.

Beamwidth: The radar beam can be as a cone and the footprint viewed as the intersection of the cone with the ground. The angular widths of beam in the azimuth and elevation planes are its two important dimensions. In each plane, the half-power

beamwidth or simply beamwidth, is defined by the angle subtended by the beam "edges," in which the beam edge is defined when the radiation strength is 3 dB below the maximum.

The beamwidth is approximately the wavelength divided by the antenna length in this direction, in azimuth with an equally driven aperture. Real strength of SAR, as the SAR moves antenna length increases, correspondingly beam squeezes and hence increase the resolution of the view/scene in azimuth direction which is not the case in elevation direction. In elevation, the beamwidth governs the width of the imaged "range swath". Since the elevation radiation pattern is usually shaped with a nonuniform aperture therefore its formula is more complicated.

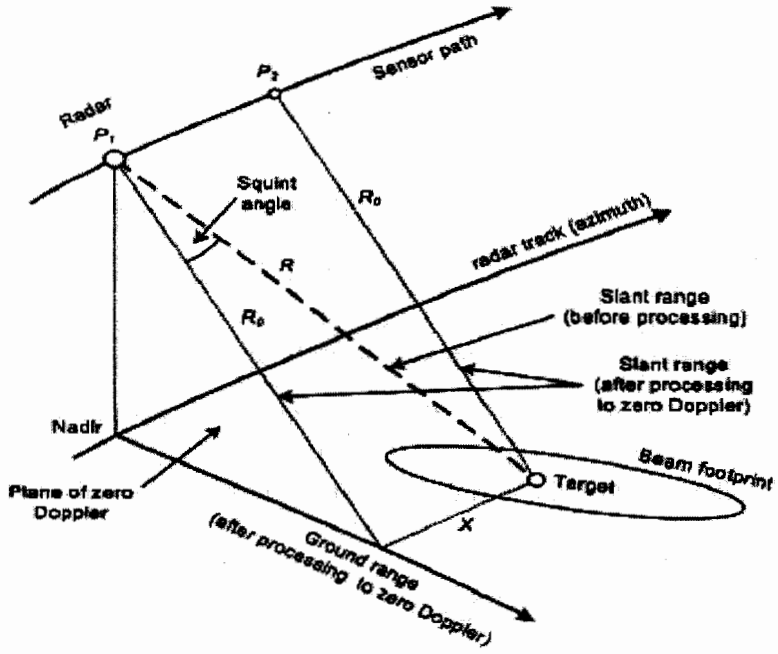

Figure 3.6: SAR data acquisition geometry

Range: First, the generic term "range" can mean slant range or ground range as shown in Figure 3.6. The earlier is measured along the radar line-of-sight, while the latter is measured along the ground. Because all SAR processing operations use the

slant range definition, the usual convention is that "range" defaults to "slant range" when not specified.

Secondly signal space and image space are two cases to consider in the definition of range. In signal space, range is a distance measured from the radar antenna to the target on the ground. It is not orthogonal to the azimuth axis unless the squint angle, as defined in Figure 3.6 is zero. This range direction is called the radar "line-of-sight". It is approximately along the beam centerline or boresight, but the direction varies with the location of the target within the beam. The image is registered to the azimuth position of closest approach and to the range of closest approach, after the SAR processing. The range axis is perpendicular to the azimuth axis at this point. Range can either be line-of-sight or orthogonal to azimuth between the various stages of SAR processing.

Slant range plane: This is the plane containing the relative (ECR) sensor velocity vector and the slant range vector for a given target. The orientation of this plane, relative to the local vertical, changes with targets at different ranges, Ro.

Ground range: This is the projection of slant range onto the ground. The slant range variable is converted to ground range if the image is to be presented in a maplike format. Ground range is the direction orthogonal to the azimuth axis and parallel to the Earth's surface with its origin at the nadir point as shown in Figure 3.6, assuming that the data is registered to zero Doppler.

Squint angle: This is the angle θsq that the slant range vector makes with the zero Doppler planes and is an important component in the description of the beam pointing direction. It is measured in the slant range plane. It coincides with the beam yaw angle

if viewed from above. For a given beam pointing direction, the squint angle depends upon the target range, Ro.

Cross range: This is a direction orthogonal to the range direction. The cross range and azimuth axes are not parallel unless the squint angle is zero. Theoretically, "azimuth" resolution is developed along the cross range axis instead of the azimuth axis. But in stripmap SAR the squint angle is usually small; the cross range resolution does not differ much from the azimuth resolution.

3.3 SAR Signal in the Range Direction

First we discuss SAR signal in the range direction because it is convenient to consider the SAR signal first in the range or beam direction, then in the azimuth direction.

3.3.1 Transmitted Pulse

In the range direction, the radar sends out an FM pulse given by [4]

$$spul(\tau) = w_r(\tau)\cos\left(2\pi\sum_{n=0}^{N} P_n \tau^n\right) \tag{3.2}$$

Where τ is the range time, and P_n are the phase coefficients, when the signal phase is expressed as a power series. The pulse envelope is usually approximated by a rectangular function

$$w_r(\tau) = rect\left(\frac{\tau}{T_r}\right) \tag{3.3}$$

Where T_r is the pulse duration. It is usually safe to assume a rectangular envelope when defining the matched filter processing even if the pulse is not quite rectangular. In early radar systems, the pulse was generated by an analog Surface Acoustic Wave (SAW) [23], but now it is generated by digital synthesizer.

The most commonly used pulse has a linear FM characteristic [4]

$$spul(\tau) = w_r(\tau)\cos\{2\pi f_0\tau + \pi K_r\tau^2\} \quad (3.4)$$

Where K_r is the FM rate (slope) of the range pulse in MHz/μsec. Here, τ is referenced to the center of the pulse for convenience. In this form, the phase coefficients are $P_0 = 0$, $P_1 = f_0$, $P_2 = K_r/2$ and $P_n = 0$ for n > 2. The instantaneous frequency of the signal $spul(\tau)$ varies with fast time τ. The instantaneous frequency is $f_i = f_0 + K_r\tau$, for a linear FM pulse given by (3.2). The radar wavelength is c/f_i so the wavelength also varies within the pulse. The pulse is said to be "up chirp" when the sign is positive because the pulse frequency increases with time. Similarly the pulse is said to be "down chirp" when the sign is negative. Due to governing the range resolution and the sampling requirements the signal bandwidth is considered a very important parameter. The pulse or signal bandwidth is given by $|K_r|T_r$. To prevent aliasing the complex sampling rate F_r of the received signal must be higher than the bandwidth during demodulation. Minimum sampling rate should satisfy Nyquist criteria. The complex sampling rate is

$$F_r = \alpha_{os,r}|K_r|T_r \quad (3.5)$$

Where K_r is the slope of range pulses and T_r shows its duration.

3.3.2 Data Acquisition

How the data are acquired across the range direction is shown in Figure 3.7 [4]. The radar beam has a certain 3-dB width in the elevation plane is called the "elevation beamwidth". The beam illuminates a section of the ground lying between "near range" and "far range" in the figure. Between the two dashed arcs in the figure, the pulse has a finite range at a given point in time.

The pulse expands outward at the speed of light in concentric spheres. The pulse at the instant it reaches the ground, at a time t_1 after it leaves the transmitting antenna is shown in Figure 3.7 by the lower dashed arc. The trailing edge of the pulse passes the "far range" point, at time t_2, a fraction of a millisecond later. In this way for duration of T_r each point on the ground, between near range and far range is illuminated. Note that at any instant, only a portion of the beam footprint is illuminated by the pulse. This portion sweeps outwards at the speed of light divided by $\sin\theta_i$ where θ_i is the local beam incidence angle. The reflected energy at any illumination instant is a convolution of the pulse waveform and the ground reflectivity (g_r) within the illuminated patch

$$s_r(\tau) = g_r(\tau) * spul(\tau) \tag{3.6}$$

Between times $2t_1$ and $2t_2$ this energy arrives back at the receiving antenna. The sampling of receiver starts a few microseconds before $2t_1$ and finishes a few microseconds after $2t_2$, thereby recording the ground reflections between near range and far range. Range ambiguities may occur if the elevation beam is too wide in relation to the interpulse period; that results from mixing of the reflected energy from consecutive pulses at the receiver [4].

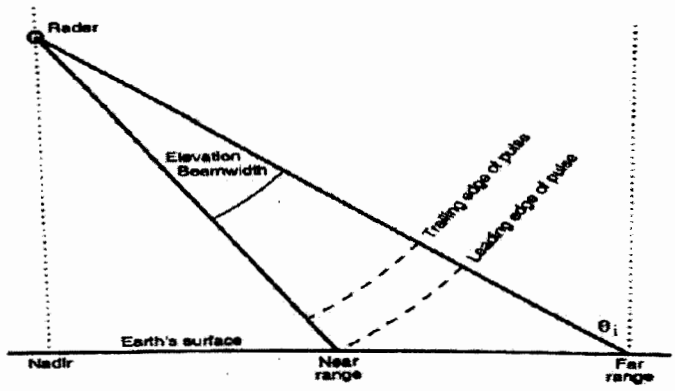

Figure 3.7: Illustrating the radar beam's 3-dB elevation beamwidth and the radar pulse spreading outward in concentric spheres.

3.4 SAR Signal in the Azimuth Direction

In the previous section, the signal received from a single pulse was discussed. As the sensor moves along its path, subsequent pulses are transmitted and received by the radar. The pulses are transmitted every **1/PRF** of a second, where PRF is the pulse repetition frequency. To discuss SAR signal in Azimuth direction we need to discuss Doppler frequency in the SAR context.

3.4.1 What Is Doppler Frequency in the SAR Context?

Data transmission in azimuth direction is shown in Figure 3.8 [4]. Consider radar that transmits a pure tone, which is generated by a local oscillator. The signal is transmitted through the antenna. The resulting electromagnetic (EM) wave travels to the ground where it strikes an object and is reflected (scattered). The reflected EM wave travels back to the antenna where it is converted into a voltage.

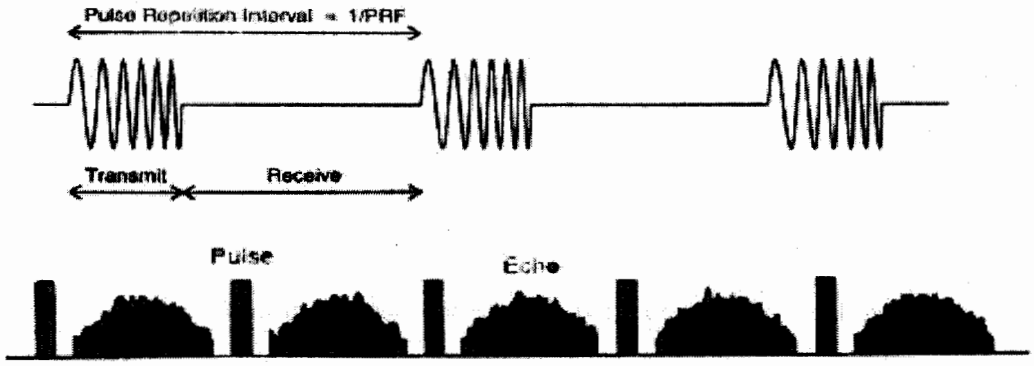

Figure 3.8: Pulse Transmission in azimuth direction

The received signal is much weaker than the transmitted signal and has a frequency shift governed by the relative speed of the antenna and scatterer. But the received signal has the same waveform as the transmitted signal. The frequency of the received signal increases if the distance from the antenna to the scatterer is decreasing. On the contrary, the frequency of received signal decreases if the distance

to the scatterer is increasing. SAR Doppler frequency is governed by the relative speed of the sensor and the target which analogous to the well-known effect in physics. This discussion gives an intuitive description of the Doppler Effect in coherent radars. If the steady timing of the local oscillator allows one to view the change in phase and frequency of the received signal very precisely, the radar is "coherent".

The following points are omitted from the above discussion:

1. The radar system generates and transmits a finite-duration pulse rather than a pure tone.
2. The radar electronics upconverts the pulse to a very high frequency and subsequently downconverts the received signal to the original frequency.
3. The pulse has a linear FM waveform rather than a tone and after reception and downconversion, it is converted to a sharp impulse which is near to the form of a sinc function.
4. The Doppler frequency is a function of the carrier frequency rather than the original baseband pulse frequency.
5. The pulses are repeated at a quite controlled time interval called pulse repetition interval (PRI). The inverse of this is the PRF.

The concept of Doppler frequency is still valid in the modulated, pulse radar, despite these simplifications in the analogy. The effect of the pulses is to sample the waveform representing the Doppler-shifted, received signal, with the sampling frequency being the PRF. The sampling of the continuous signal creates an aliasing effect when the Doppler frequency exceeds the sampling frequency. It is the

sampling that strongly affects how the Doppler frequency is observed and how it is projected.

3.4.2 Doppler Bandwidth

Consider Figure 3.9 as the radar moves it passes through the point targets at point B and D as shown. The Doppler shift will vary approximately linearly with time, passing the zero frequency at boresight for zero squint. This Doppler shift approximates to linear chirp. Azimuth compression can be thought of as the compression of the Doppler signal produced during the integration length, $R\emptyset_a$. As the platform moves past the targets, the Doppler bandwidth consist of the frequencies produced as a result of scatterers falling in the beamwidth of the radar. For narrow azimuth beamwidth the Doppler bandwidth is given by [23]

$$fd_2 - fd_1 = \frac{2v_p\emptyset_a}{\lambda} \tag{3.7}$$

where $\emptyset_a$ is 3-dB beamwidth and v_p is the platform ground velocity. Nyquist Sampling in SAR mode requires that,

$$PRF \geq \frac{2v_p\emptyset_a}{\lambda} \tag{3.8}$$

To avoid undersampleing and aliasing in processing of the cross range data we set a minimum Pulse Repetition Frequency (PRF).

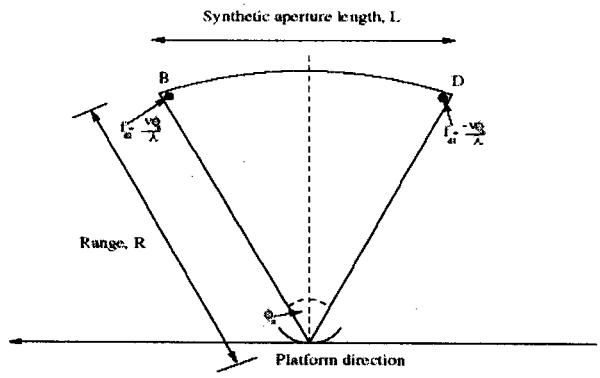

Figure 3.9: Stationary Point Target in moving Radar Beam.

3.5 The Two-Dimensional Signal

This section includes the configuration of received radar signal as a two-dimensional signal within the signal processor and range cell migration.

3.5.1 Data Arrangement in Signal Memory

The received radar signal is one-dimensional, in simple sense a voltage as a function of time. The waveform of the received signal could take the form as shown in Figure 3.10, in accordance to the transmit/receive cycles. Each segment represents the ground echo received during one pulse cycle. The time for which receiver is turned off is shown by the gaps between each segment, the time also includes the pulse transmission time plus an allowance for switching of the signal paths. The format of the signal in Figure 3.10 is how it might appear in a one-dimensional storage media, such as magnetic tape.

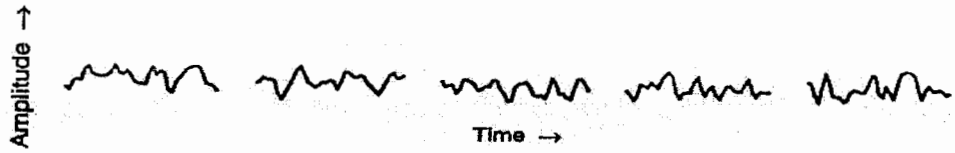

Figure 3.10: Amplitude or Voltage of the received radar signal

Consider the Figure 3.11 to show the radar received signal as a two dimensional signal [4]. For simplicity assume that the radar beamwidth is finite in azimuth. The target is just entering the radar beam when the sensor is at point A. The received signal from the target which is part of the echo from a given transmitted pulse is written into one row of SAR signal memory. For the time being this memory may actually be on tape or in downlink memory, it can be considered as being in the memory at the input to the SAR signal processor.

More pulses are transmitted as the sensor advances and the associated echoes are written into successive rows in the signal memory. The target leaves the beam when the sensor is at point B and the last received energy of that target is written into SAR signal memory. Naturally memory contains data from many targets, not just one as shown in Figure 3.11. In practice the azimuth beamwidth is not finite which means that energy received from the azimuth sidelobes from each target is also recorded before A and after B.

Consider "one-dimensional" signal as shown in Figure 3.10, one can also think of this format as a two-dimensional. Where the received signal is sampled and written into a computer memory as shown in Figure 3.11. The data from each segment or pulse are written into a new row in memory. The beginning of each row with respect to the pulse transmission time occurs at a fixed time delay. In this way in Figure 3.11 the horizontal axis represents the travel time τ or range from the sensor to the ground. From another aspect, one can consider a single column in Figure 3.11 in which each sample corresponds to the same range from the sensor. A row is sometimes called a range line and a column is called a range gate [4].

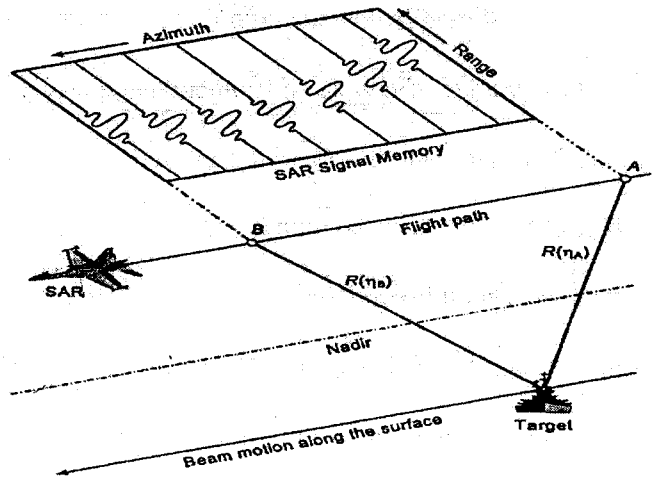

Figure 3.11: How the received SAR data are placed in a two-dimensional signal memory.

Now consider the vertical axis of Figure 3.12 [4] of the two-dimensional memory. The sensor has moved a small amount in the azimuth direction from one sample to the next, while each sample in a given column is at the same range. So this vertical axis can be labeled "azimuth" or azimuth timeη. As the objective is to make a two-dimensional image of the Earth's surface, data have now been recorded corresponding to two near-orthogonal directions on the Earth's surface.

One can see in this way that how a two-dimensional signal with the coordinates being range time and azimuth time is obtained from the radar system. The azimuth time is also called "slow time" and the range time is called "fast time". Because the azimuth distance is related to azimuth time by the much slower forward motion of the beam footprint and the range distance is related to range time by the speed of light.

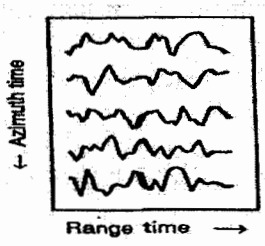

Figure 3.12: How the voltage of the received radar signal of Figure 3.10 is written into the two-dimensional signal processor memory.

To summarize, the radar samples are written along the horizontal range axis, these samples are originated from the sampling of a continuous-time analog signal. In the azimuth direction the signal is naturally in discrete-time from the outset. In the two-dimensional signal memory the azimuth samples are written along the vertical azimuth axis.

3.5.2 Range Cell Migration

The instantaneous slant range, $R(\eta)$, changes with azimuth time, η according to

$$R^2(\eta) = R_0^2 + V_r^2\eta^2 \tag{3.9}$$

In which $R(\eta)$ is expressed as a hyperbolic function of η. The equation represents the target trajectory as a function of azimuth time in distance units. The separation between range samples is $c/(2F_r)$ where F_r the range is sampling rate. This means that the trajectory migrates through range cells during the exposure time of the target in signal memory, hence the name "range cell migration" or RCM. This migration complicates the processing but ironically, it is an essential feature of SAR [4].

CHAPTER 4 ANALYSIS OF SAR DESIGN PARAMETERS

The system design process consists of two parts; the first part being the hardware design that includes the design and selection of main parameters of the SAR system. The second part being software design which is covered in Chapter no.7 Simulation & Results which includes the development of signal processing techniques to analyze and display the data and formulate an image. This chapter partially addresses the first part.

4.1 Proposed Design Consideration

While designing any SAR system we should keep in mind the following parameters and ranges.

4.1.1 Operating Frequency and polarization

Frequency range from 1 to 30 GHz is normally used for remote sensing application. The transmissivity through air approaches 100% in the 1-10 GHz range. In this frequency range SAR is always able to image the earth's surface independent of the cloud cover or precipitation. For X-band SAR we use 9.6 GHz which is within the allowable spectrum (9.5G-9.8GHz) defined by International Telecommunication Union (ITU) for Earth Exploration Satellite System (EESS) [24].

4.1.2 Modulation and Mode of Operation

Modern radar uses chirp or Linear Frequency Modulation (LFM) to increase range resolution when long pulses are required to get reasonable signal to noise (S/N). The same average transmitting power as in a pulse system can be achieved with lower peak amplitude. The LFM gives better sensitivity without

sacrificing range resolution and is easy to implement. The lower peak power allows for the use of commercially available microwave components that have moderate peak power handling capability.

Stripmap is standard mode of SAR operation which is widely used by airborne SAR sensors where a strip to the side of the aircraft is imaged. The radar antenna pattern is oriented towards the ground, orthogonal to the flight track and to one side of aircraft. A swath is mapped out on the ground by antenna footprint as the aircraft moves.

4.1.3 Resolution and Swath Width

Typical resolution of airborne SAR range from 1 m to 20 m. It depends mostly on the application requirements [25].

4.1.4 Operation Platform and Antenna

A small aircraft flying or other suitable aerial platform at low altitude will be used in order to achieve low cost SAR design. The SAR system should support true ground speed at 100m/s and operating altitude of at least 1000m. A typical airborne SAR antenna has the gain of 17 dB to 28 dB.

4.1.5 Range of Incident Angle

From the open literatures the incident angle from 0 to 90 degree is utilized by present airborne SARs. The backscattering coefficient of nature targets such as soil, grass and vegetable are maintained almost constant over the incident angle of 40 to 60 degree [26, 27].

4.1.6 Dynamic Range of Backscattering Coefficient

The required system sensitivity is determined based on various categories of earth terrain to mapped such as man made target, ocean, sea-ice, forest, natural vegetation and agriculture, geological targets, mountain, land and sea boundary. From open literatures the typical value of dynamic range of backscattering coefficient falls in the range of +20 dB to - 40dB. For vegetation the typical value of dynamic range of backscattering coefficient vary from 0 dB to – 20 dB [28, 29].

4.2 Design parameters Study for SAR System

Table 4.1 shows comparison of different parameters of some early small scale SAR systems.

Parameter	**Mini SAR**	**Lynx:SAR**	**BYE μSAR**	**YSAR**	**IMSAR**
Weight	<50Kg	120lb	2Kg	no-info	1 to 2 lb
Volume	COTS pod of length 19″	no-info	1ft in length	no-info	6.2x7.5x4.5 in-cube
Power consumption	<1.5KW	320W	18-20W	18-20W	10-25W (15W)
Data storage	On-board	no-info	1GB		32GB
antenna	Phase array	Horn fed dish antenna	patch array	patch array	
SAR Mode					
Resolution	<0.5m	0.3m	0.15m	0.8m	14x14 in
Swath	>2Km	10Km	no-info	no-info	no-info
Center Frequency	X-band	Ku-band	5.56 GHz	2.1GHz	X-band
SAR processing	Off-line	-	no-info	no-info	on Board & Real Time
Range	>7Km	7 to 30Km	<300m	2000ft	3300ft=1km

Table 4.1: Design parameters Study for SAR System

The primary goal of this thesis is to prepare feasibility report for developing an indigenous SAR system. High level system design and subsystem level

requirements have been carefully considered, a comparison of these parameters for different international SAR system is presented. Below is the explanation of the important parameters listed in Table 4.1 and some other parameter related to SAR design.

4.2.1 Altitude\Range

SAR is usually side-looking imaging radar which means that the radar antenna beam is pointed sideways, typically nearly perpendicular to the flight direction of the platform. As depicted below, Figure 4.1 illustrates the basic side-looking geometry. The transmitted pulses is reflected from targets, or scatterers, located at increasing distances from the radar along the ground as they propagate from the radar. One line of SAR data as a function of the time delay to the scatterers is formed by the received echoes from a single transmitted pulse. Thus range in a radar image is the distance from the radar to the scatterer. This is not the same as distance along the ground, since the radar is located at some altitude above the ground. Thus the dimension in the image is called slant range which is opposed to ground range, as shown in the Figure 4.1 [30].

The radar transmits pulses and receives echoes periodically. A pulse is transmitted at different locations along the flight path as the platform is moving. Thus, the other dimension in the radar image is the azimuth, or along-track direction. In order to assume that the echo of the pulse from the ground is to be received at the same platform position at which the pulse was transmitted, the speed of light at which the pulse propagates is much faster than the spacecraft velocity. The resolution of the image in the range direction is dependent on the length of the emitted pulse, shorter pulses result in finer resolution.

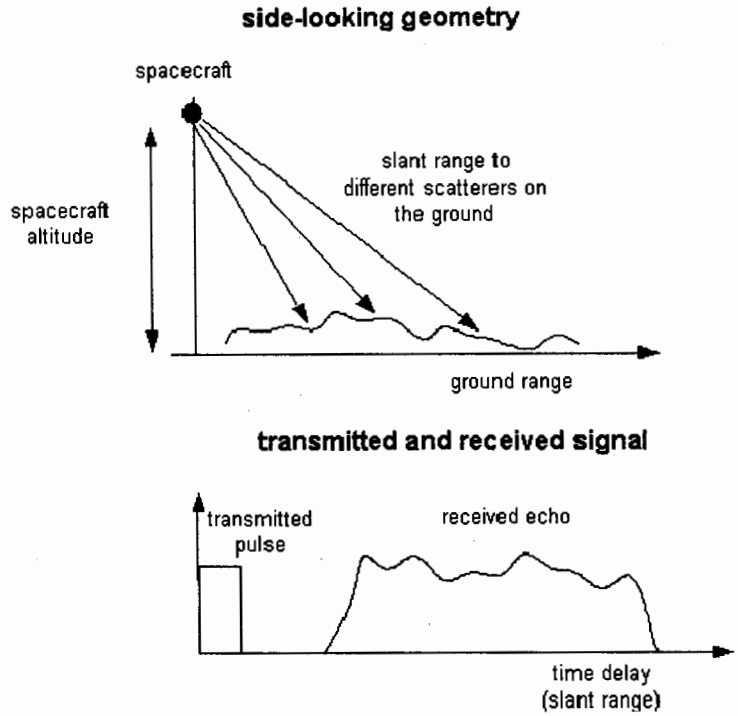

Figure 4.1: Side-looking radar geometry and slant range dimension in line of SAR data.

4.2.2 Frequency

Frequency can be defined as rate of oscillation of a wave or number of oscillations per unit time or number of wavelengths that pass a point per unit time. This term is most often used with radar in remote sensing. The frequency bands were first designated by letters for military secrecy which were used by radars. The product of wavelength and frequency is equal to the speed of propagation, for electromagnetic waves, which, in free space, is the speed of light. Frequencies are on the order of 0.3 GHz-300 GHz, having wavelengths of 1mm - 1 m respectively, in the microwave region [31]. Typical microwave frequency bands are listed in Table 4.2. The common microwave bands used in radar applications are shown in Table 4.3 [32].

Microwave Frequency Bands		
Band	**λ (mm)**	**F (GHz)**
Ka	8-11	40-26.5
K	11-17	26.5-18
Ku	17-24	18-12.5
X	24-38	12.5-8
C	38-75	8-4
S	75-150	4-2
L	150-300	2-1
P	300-1000	1-0.3

Table 4.2: Typical microwave frequency bands

Mission	Country	Band	Time
SEASAT	USA	L	1978
ERS-1	Europe (ESA)	C	1991-2000
J-ERS-1	Japan	L	1992-1998
SIR-C/X-SAR	USA	L, C, X	1994
Radarsat-1	Canada	C	1995
ERS-2	Europe (ESA)	C	1995
SRTM	USA	C, X	2000
ENVISAT ASAR	Europe (ESA)	C	2002
ALOS PALSAR	Japan	L	2005
TerraSAR-X	Germany	X	2006
SAR-Lupe	Germany	X	2006
CosmoSkymed	Italy	X	2006
Radarsat-2	Canada	C	2007

Table 4.3: Space-borne SAR mission using different bands

4.2.3 Polarization

Microwaves are transversal waves which mean that in the direction of propagation the electric and magnetic fields are mutually orthogonal. The polarization component is defined by the electric field vector. A planar (or linear) polarization refers to the vibration of the electric field vector in a parallel direction to the propagation wave. There are also elliptical and circular polarizations which are characterized by the rotation of the electric field vector in corresponding fashion.

Most of the radar systems use linear polarizations which are operating using vertically or horizontally polarized microwave radiation. There are four combination of linear polarization which include like-polarized (HH, VV) and cross-polarized (HV, VH). Depending on the polarization of transmitted wave the targets on the Earth's surface scatter microwave radiation differently. The like-polarized backscatter is stronger, For instance, a wheat field has a dominant vertical component, so the interaction and backscatter with a VV polarized wave is much stronger than that a HH wave. SAR system with cross-polarized receiving capabilities can provide additional information for the image interpretation and understanding the target/wave interaction.

4.2.4 Swath Width

The swath width is a parameter which is dependent on along track resolution, platform velocity and off-nadir angle. Two radar pulse returns must not be received simultaneously from the illuminated footprint (instantaneous field of view, IFOV) of real aperture antenna.

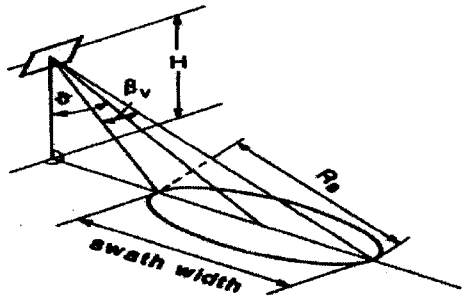

Figure 4.2: Distance between two pulses must be greater than $2R_s$ in order to avoid range ambiguities occurring within the IFOV.

Considering Figure 4.2, we notice that the slant range differences between the edges of the illuminated swath width is given by the slant swath width

$$R_s = \frac{H\beta_v \sin\theta}{cos^2\theta}$$

Where R_s slant range swath width, H is the altitude of the antenna above the ground and β_v is azimuth half power beam width [33].

A trade-off between resolution and swath width can be enforced by the estimated minimum dimensions of the real antenna. We can achieve high resolution only with a small swath width, increasing the swath width reduces resolution. Figure 4.3 shows a small swath width enforces a long synthetic aperture and high resolution while Figure 4.4 shows a wide swath width cause low resolution and a short synthetic aperture [33].

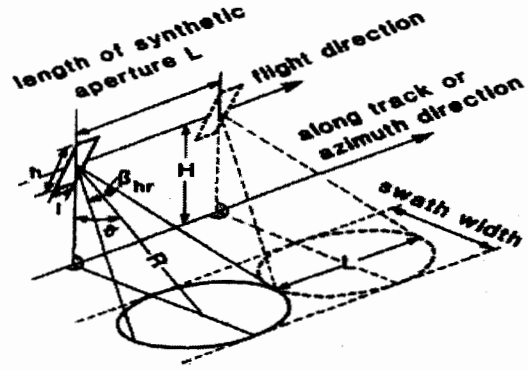

Figure 4.3: A small swath width enforces a long synthetic aperture and high resolution

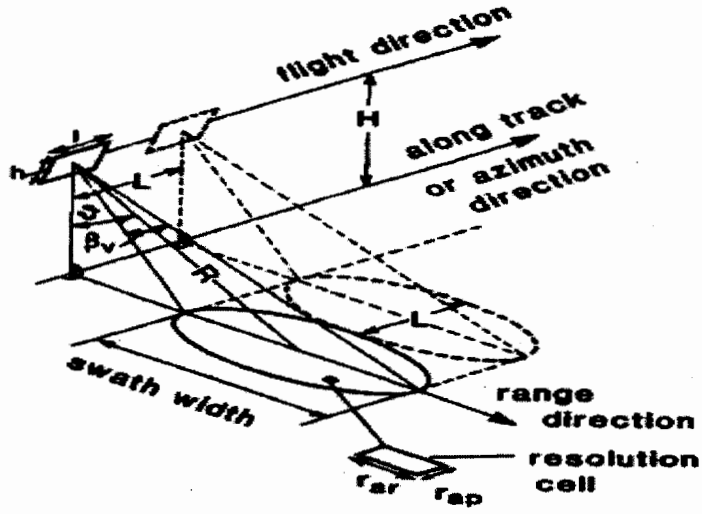

Figure 4.4: A low resolution corresponds to a short synthetic aperture and a wide swath width.

4.2.5 Nadir

The nadir is the point on the Earth's surface directly below the sensor, so that the "normal" to the Earth's surface at the nadir passes through the sensor. The vector from the sensor to the Earth's center intersects the Earth's surface at the nadir for a spherical Earth model. For an ellipsoidal model this is not true [4].

4.2.6 Ground range

The projection of slant range onto the ground is called ground range. The slant range variable is converted to ground range if the image is to be presented in a maplike format. Ground range is the direction orthogonal to the azimuth axis and parallel to the Earth's surface, with its origin at the nadir point, assuming that data is registered to zero Doppler [4].

4.2.7 Pulse Repetition Frequency (PRF)

In the aircraft case the platform velocity is lower and the beam geometry restricts the swath width to well below the ambiguity limit. This means that the PRF can be made higher than that needed to sustain the azimuth bandwidth. A higher PRF without raising the peak power or the pulse length allows the transmission of a higher average power, thereby improving the SNR. When this occurs, to increase the efficiency of subsequent processing steps, the azimuth signal can be filtered and the sampling rate reduced. This filtering and sample rate reduction is called "presuming" which lowers the PRF, resulting in more efficient SAR processing [4].

The Nyquist sampling theorem requires a pulse repetition frequency (PRF) equal to or higher than the Doppler frequency shift f_D which is used in SAR processing per channel. Generally a PRF of 1 to 1.3 times f_D will be chosen.

To control range ambiguities [38] we need

$$PRF < c/(2W_g \sin\eta) \tag{4.1}$$

Where PRF is the pulse repetition frequency and c is the speed of light. The PRF must be smaller than the time it takes to collect returns from the entire illuminated swath. To avoid azimuth ambiguities the PRF should be

$$PRF > B_D \tag{4.2}$$

Where B_D is Doppler bandwidth. B_D is the range of Doppler frequencies extending across the antenna footprint. Generally the Doppler bandwidth is given as:

$$B_D = 2V_{st}/L_a \tag{4.3}$$

Where L_a is the antenna length and V_{st} is the velocity.

The upper limit on the PRF, given in equation (4.1) is independent of the squint angle. Thus in selecting the PRF lies in the lower limit we may have any flexibility which seeks to control azimuth ambiguities caused by Doppler aliasing [34].

4.2.8 SAR Antenna

In SAR systems currently two basic antenna technologies are used. One is a constrained (corporate) feed array (planar or modified planar). This system can be pointed electronically although some mechanical redirection may also be incorporated. Space Shuttle SAR (SIR-A and SIR-B), ALMAZ, SEASAT, ERS-1, ERS-2, JERS-1 and RADARSAT-1 are examples [35].

Second technology is a distributed array using transmit/receive that is similar in electrical performance to the corporate feed array. Better phase control and beam steering are the advantages of this system. These systems were first introduced by Space Shuttle SIR-C and STRM designs and are the basis for the ENVIST and RADARSAT-2 designs [35].

4.2.9 Antenna Gain

The degree to which an antenna concentrates electromagnetic energy in a narrow angular beam is described by antenna gain. The directive gain and directivity are the two parameters associated with the gain of an antenna.

At a far-field distance, R, the directive gain, G, is defined as the ratio [36]

$$G = \frac{\text{maximum radiation intensity}}{\text{average radiation intensity}}$$

$$= \frac{\text{maximum power per steradian}}{\text{total power radiated}/4\pi}$$

This ratio can also be expressed in terms of maximum radiated power density at a far-field density, R, over the power density radiated by an isotropic source at that same distance [36]

$$G = \frac{\text{maximum power density}}{\text{total power radiated}/4\pi R^2}$$

$$= \frac{P_{max}}{P_{rad}/4\pi R^2} \tag{4.4}$$

The value of the directive gain in the direction of its maximum value is the definition of directivity D_{max}. The gain of antenna is related to the directivity is given by [36]

$$G = \epsilon \, D_{max}$$

Where $\in$ is the radiation efficiency which is given by

$$\epsilon = \frac{P_{rad}}{P_{tx}} = \frac{P_{tx}}{P_{tx} + P_{loss}} \tag{4.5}$$

Where P_{rad} is the actual power being radiated and P_{tx} is the power coupled into the antenna.

4.2.10 Chirp Bandwidth

Due to quadratic phase of a linear FM signals its frequency is a linear function of time. The frequency slope is the linear FM rate. A linear FM signal is frequently called a "chirp" in analogy with a bird's call. The signal is called "up chirp" when the slope is positive and called "down chirp" when the slope is negative [4].

To achieve the desired chirp bandwidth (range resolution) the bandwidth of the antenna should be broad enough to easily achieve the required level. Outside the useful bandwidth the frequencies (signals) should be rejected or at least strongly attenuated. A relative bandwidth of 3 % to 5 % is attained by typically microstrip and wave guide array. Therefore, it is advisable to use higher frequency bands for the SAR to achieve high slant range resolution, r_R. Slant range resolution is defined by [33].

$$r_R = \frac{c}{2B}$$

Where c is the speed of light and B is chirp bandwidth. Therefore slant range is inversely proportional to bandwidth, an increase in bandwidth will decrease r_R and thus improve range resolution.

4.3 Typical Radar Parameter Values

The set of SAR parameters values for both a spaceborne and an airborne case is shown in Table 4.4 [4]. A generic X-band system with a 1-m antenna is considered for the aircraft case. Those parameters which affect range processing and which mainly affect azimuth processing is separated in the table. In the satellite case the squint is caused by Earth rotation assuming no yaw steering. The squint in the airborne case is caused by side winds and physical antenna motion [4].

Parameter Name	Symbol	Aircraft	Satellite	Units
Range Parameters				
Slant range of scene center	$R(\eta_c)$	30	850	Km
Altitude		10	800	Km
Transmitted pulse duration	T_r	10	40	μs
Range FM rate	K_r	10	0.5	$MHz/\mu s$
Signal bandwidth		100	20	MHz
Range sampling rate	F_r	120	24	MHz
Slant range swath width		10	50	Km
Azimuth Parameters				
Effective radar velocity	V_r	250	7100	m/s
Radar center frequency	f_0	9.4	5.3	GHz
Radar wavelength	λ	0.032	0.057	M
Azimuth FM rate	K_a	131	2095	Hz/s
Synthetic aperture length	L_s	0.85	4.8	Km
Target exposure time	T_a	3.4	0.64	Sec
Antenna length	L_a	1	10	M
Doppler bandwidth	Δf_{dop}	443	1338	Hz
Azimuth sampling rate(PRF)	F_a	600	1700	Hz
Squint angle	$\theta_{r,c}$	< 8	< 4	deg.

Table 4.4: Representative Spaceborne and Airborne SAR Parameters

Following is the explanation of different parameters listed in Table 4.4.

4.3.1 Range Parameters

This section includes Slant range of scene center, Transmitted pulse duration, Range FM rate, Signal bandwidth and Range sampling rate as mentioned in Table 4.4.

4.3.1.1 Slant range

In general the target is illuminated by the beam center at a "beam center crossing time" η_c, referenced to the time of zero Doppler, in the nonzero squint case. Where η_c is negative, when the beam squints forward. Conversely η_c is positive when the antenna squints backward. The time, η_c is given by [4]

$$\eta_c = -\frac{R_0 \tan \theta_{sq,c}}{V_g} = -\frac{R(\eta_c) \sin \theta_{sq,c}}{V_g} \tag{4.6}$$

Where $R(\eta_c)$ is the slant range to the target at the time it is illuminated by the beam center and $\theta_{sq,c}$ is the value of θ_{sq} at this time. Where V_g represents the smallest velocity.

4.3.1.2 Transmitted pulse duration

The pulse envelope is usually approximated by a rectangular function

$$w_r(\tau) = rect\left(\frac{\tau}{T_r}\right)$$

Where T_r is the pulse duration. It is usually safe to assume a rectangular envelope when defining the matched filter processing even if the pulse is not quite rectangular. In early radar systems, the pulse was generated by an analog Surface Acoustic Wave (SAW) [37], but now it is generated by digital synthesizer.

4.3.1.3 Range FM rate

The choice of the sign of the FM rate is up to the system designer. The pulse is said to be "up chirp" when the sign is positive because the pulse frequency increases with time. Similarly the pulse is said to be "down chirp" when the sign is negative. The structure of SAR processing and the quality of the processed image are not affected by the direction of the chirp.

4.3.1.4 Signal bandwidth & Sampling Rate

Due to governing the range resolution and the sampling requirements the signal bandwidth is considered a very important parameter. The pulse or signal bandwidth is BW = $|K_r|T_r$ [4] given by$|K_r|T_r$. To prevent aliasing the complex sampling rate F_r of the received signal must be higher than the bandwidth during demodulation. The range oversampling ratio$\propto_{os,r}$ is the sampling rate divided by the signal bandwidth. In practice it is usually between 1.1 and 1.2.

$$F_r = \alpha_{os,r}|K_r|T_r$$

4.3.2 Azimuth Parameters

In this section we will discuss important parameters in azimuth direction as mentioned in Table 4.4 which includes Effective radar velocity, Azimuth FM rate, Synthetic aperture length, Target exposure time, Doppler bandwidth and Azimuth sampling rate (PRF).

4.3.2.1 Effective radar velocity

The hyperbolic form of the range equation is given by

$$R^2(\eta) = R_0^2 + V_r^2\eta^2 \tag{4.7}$$

where η is the azimuth time referenced to the time of closest approach and R_0 is the slant range when radar is closest to the target that is, R_0 is the range of closest approach.

The hyperbolic range equation holds for a satellite with this assumption, except that V_r is not a physically velocity but a pseudovelocity. The parameter V_r has been called the "radar velocity," effective velocity," or "speed parameter" by several authors [38]. A better term may be "effective radar velocity," although some authors prefer not to call it velocity at all [39].

Variation of V_r with range and also varies slowly with azimuth as the satellite orbit and the Earth rotation component changes is the important differences from the aircraft case. Its numerical values lie between the satellite platform velocity V_s and the lower speed V_g with which beam moves along the ground. The hyperbolic model is adequate over the duration of the target exposure time, which is typically on the order of second. An approximation for V_r is

$$V_r \approx \sqrt{V_s V_g} \tag{4.8}$$

Variation of V_s and V_g related with orbit position and range because the magnitude of the Earth's tangential velocity changes with latitude as well as its direction related to the satellite velocity vector. In this way the variation of V_r is with time and range and must be updated around the orbit. The above approximation mainly comes from the fact that orbit is not circular.

In precision SAR processing the above approximation is not accurate enough for calculating the azimuth matched filter coefficients. It is adequate for

analysis purposes such as finding the exposure time and Doppler bandwidth. A refined geometric model is used for calculating V_r for precision SAR processing. V_r and V_g are varying with range so they are calculated at zero Doppler point of the target and they don not vary along the target exposure as they are function of R_0. That means V_r is a constant for a particular point target, an important fact to note in a point target simulator.

The selection of appropriate velocity, depend upon the application. As V_r is the velocity used to obtain the Range Cell Migration and the azimuth FM rate in the azimuth SAR processing and V_s is used to obtain Doppler bandwidth. Finally V_g is used for ground resolution and ground distance.

4.3.2.2 Azimuth FM rate

The rate of change of azimuth or Doppler frequency is the Azimuth FM rate [4].

$$K_a = \frac{2}{\lambda}\frac{d^2R(\eta)}{d\eta^2}\bigg|_{\eta=\eta_c} = \frac{2V_r^2\cos^2\theta_{r,c}}{\lambda R(\eta_c)} = \frac{2V_r^2\cos^3\theta_{r,c}}{\lambda R_0} \tag{4.9}$$

Where the azimuth frequency is $2/\lambda$ times the first derivative of range.

4.3.2.3 Synthetic aperture length

Synthetic aperture length is shown by L_s in Figure 4.5. It is the path length of the sensor during the time that a target stays within the radar beam.

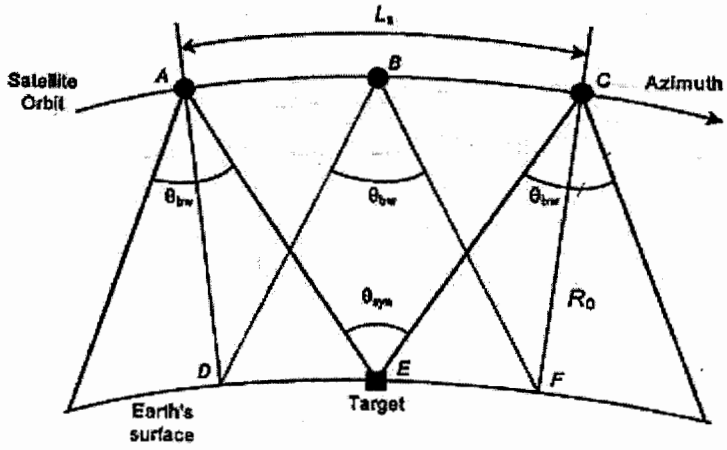

Figure 4.5: Antenna azimuth beamwidth and Synthetic angle & length

The amount of data that is available for processing from a given target is governed by this length. The synthetic aperture is given by [4]

$$L_s = \frac{R_0\,\theta_{bw}}{\cos\theta_{r,c}}\frac{V_s}{V_g} = \frac{0.866R_0\lambda}{L_a\cos\theta_{r,c}}\frac{V_s}{V_g} = \frac{0.866R(\eta_c)\lambda}{L_a}\frac{V_s}{V_g} \qquad (4.10)$$

Where $\theta_{bw} = 0.866\,\lambda/L_a$ and the ratio V_s/V_g is due to the difference between the beamwidth and synthetic angle.

4.3.2.4 Doppler bandwidth

Considering equation of Doppler centroid the azimuth bandwidth of the target can be derived as [4]

$$\Delta f_{dop} = \left|\frac{2V_r\cos\theta_{r,c}}{\lambda}\frac{V_g}{V_r}\,\theta_{bw}\right| = \frac{2V_g\cos\theta_{r,c}}{\lambda}\,\theta_{bw} \qquad (4.11)$$

In which the scaling factor V_s/V_r is due to rectilinear geometry assumption. This equation makes use of the fact that bandwidth is the frequency excursion experienced by the target during the time in which the target is illuminated by the 3-db width of the radar beam $\theta_{bw} = 0.886\,\lambda/L_a$. Therefore the Doppler bandwidth is

$$\Delta f_{dop} = 0.866 \frac{2V_s \cos\theta_{r,c}}{L_a} \tag{4.12}$$

This bandwidth governs the sampling requirement that is; it defines the lower limit of the PRF. At the beam edges defined by θ_{bw} the signal strength is only down by 6 dB and the azimuth spectrum rolls off slowly. To reduce azimuth ambiguity power an oversampling factor 1.1 to 1.4 is usually used. The PRF is set to the oversampling factor multiplied byΔf_{dop}.

4.3.2.5 PRF

The PRF is selected by considering the following parameters and criteria:

1. Nyquist sampling rate: The PRF corresponds to a complex sampler as it should be larger than the significant azimuth signal bandwidth. The azimuth oversampling factor $\alpha_{os,a}$ is usually about 1.1 to 1.4. Azimuth ambiguities caused by aliasing will be troublesome if the PRF is too low.

2. Range swath width: The sampling window can be up to $1/\mathrm{PRF} - T_r$ seconds long corresponding to a slant range interval of $(1/\mathrm{PRF} - T_r)c/2$ meters. To illuminate all or most of the near range to far range interval by beam falls within the receive window, the PRF should be low enough. Range ambiguities occur because of echoes from different pulses overlapping in the receive window, if the PRF is too large in relation to the echo duration. The antenna's elevation beamwidth can be reduced by making the antenna wider or by adjusting the antenna weighting, if the range ambiguities are too large and the PRF cannot be lowered.

3. Nadir return: Sometimes bright streak in the image caused by a significant amount of energy arises from ground reflections at the nadir point. This nadir return is

bright due to occurrence of specular reflections, when the incident angle is small; each cell covers a large area. This energy is unwanted in satellite SARs, since it is range ambiguities. And it is usually possible to choose a PRF for which the nadir return does not fall within the receive window.

CHAPTER 5 LITERATURE REVIEW

5.1 Review of SAR Developments

The chapter starts with a brief history about early SAR developments and designing parameters of different early SAR programs. In 1951, Carl Wiley developed a technique for greatly expanding and improving the resolution of radar-generated images called synthetic aperture radar (SAR) with a team at Goodyear Aircraft Corporation (later Goodyear Aerospace) [40]. A synthetic aperture radio telescope was developed by Martin Ryle in 1952 based on idea of tomography [41]. In 1959, the institute's twin-engine Convair 580 was developed having a conventional cockpit, two high-resolution cameras and synthetic aperture radar, which penetrated clouds, foliage and even the ground [42]. Alpha Regio was the first feature on Venus to be identified from earth-based radar in 1963 [43]. In Hurricane Gloria a High-altitude, airborne, L-band synthetic aperture radar (SAR) data were collected on 28 and 30 September 1976 [44]. In June 1978 SEASAT-A was launched; the first spaceborne Synthetic Aperture Radar data was made available to the remote sensing community [45]. In 1981 Shuttle imaging Radar (SIR-A) series was launched for non-real time optical processing on ground. CV-580 aircraft of the Canada Centre for Remote Sensing collected C-band synthetic aperture radar (SAR) data in March 1989 over the marginal ice zone off the east coast of Newfoundland during the Labrador Ice Margin Experiment (LIMEX) [46]. NASA's launched Magellan from the Space Shuttle Atlantis on April 27, 1989 next mission to Venus. The JPL-managed spacecraft will relay high- resolution maps of Venus using synthetic-aperture radar to pierce the planet's thick cloud cover [47]. The ERS-1 satellite which was launched in July 1991, owned and operated by the European Space Agency, a group of 13

European countries. It was designed to produce images and other data on the ocean temperature, ocean surface, ocean bottom in shallow coastal areas, ice conditions, wave patterns, forest management and crop development [48]. Spaceborne Imaging Radar-C/X-band Synthetic Aperture Radar (SIR- C/X-SAR) was launched on April 10, 1994, onboard the space shuttle Endeavour [49].

In the past, many organizations, universities and researchers have studied and documented the design and development of UAV based SAR. Some of these researchers have also analyzed the effect of changing parameters and changing modes of operation. The purpose of the thesis is to design a monostatic SAR system for light aircraft and UAV applications. Therefore, it will be prudent to discuss some similar systems that have been prepared by various universities, organizations and institutes.

5.2 Review of Early Airborne SAR Systems

For frequent observation repetition and the low cost requirements airborne systems are much more appropriate for both requirements. Airborne radars are comparatively less expensive than space-borne systems. Particularly both long endurance high altitude Unmanned Air Vehicles (UAV's) as well as low flying Remotely Piloted Vehicles (RPV) are preferable platforms besides conventional aircraft. For reliable, long endurance, high altitude, standoff image collection capabilities, a conventional air vehicle has been designed by Global Hawk which was funded by the Defense Airborne Reconnaissance Office (DARO) and managed by the Defense Advanced Research Projects Agency (DARPA) and the US Air Force. Dark Star is a highly HAE UAV version, survivable, reconnaissance asset capable, operating in high air defense threat situations where assured coverage is more

important than range and endurance. The SAR can be carried by UAV's with the observation capability of about 100 000 kilometer square per day. However the large figure of airborne platforms requires for a large number of light weight and low cost SAR. There exists a very large fleet of airborne SAR-Systems (Kramer, 2000) Examples for airborne SAR with principle Polarmetric and interferometric capability are E-SAR (DLR), Do-SAR (EADS), Ramses (ONERA), AES (FGAN), SAR-580(CCRS). Table 5.1 shows some specifications [50] of these systems.

Early Airborne SAR Systems		
Instrument (Agency), Country	**Frequencyx (Baud /GHz)**	**Polarization**
C/X-SAR-(CCRS), Canada	5.3/© 9.25/(X)	C: Full polarimetric, X: V or H
DO-SAR (EDAS), Germany	3.2/(S) 5.3/© 9.6/(X) 35/(Ka)	Full polarimetric
EMISAR-(EMI/TUD), Denmark	5.3/© 1.4/(L)	Full polarimetric
E-SAR-(DLR), Germany	0.450/(P) 1.3/(L) 5.3/© 9.6/(X)	P+L: Full polarimetric C: VV or HH X: V or H
AER-(FGAN), Germany	X	Full polarimetric One pass Interferometry
MMW-SAR-MIT	33.56/(Ka)	V, H, Full polarimetric
NASAR-(NASDA/EORC), Japan	1.291 (L-Band)	Full polarimetric
P-3/SAR-ERIM, Navy, US	0.350/(UWB) 1.25/(L) 5.30/© 9.35/(X)	Full polarimetric
PHARUS-(TNO-FEL), Netherlands	5.25/©	Full polarimetric
PI-SAR-(CRL, NASDA), Japan	9.55 (X), 1.27 (L)	X: Full polarimetric
RAMSES-(ONERA), France	1.6/(L), 3.0/(S), 6.2/©, 9.5/(X), 14.5/(Ku), 35/(Ka), 95/(W)	Full polarimetric

Table 5.1: Overview of some early airborne SAR systems

Some high endurance UAV's operate above 12000 meters to avoid commercial traffic and reduce turbulence. From a conventional airport they normally operate in a variety of weather conditions. They are able to maintain a flight path with positional accuracy of ± 5 meters, have a minimum range capacity of 2000 nautical

miles, a payload capacity of 300 kg with volume of 1 cubic meter. They have 2000 watts of DC power available for the payload as a minimum, support over-the-horizon up-and downlinks for communication and data transmission. They are able to mount an external, side-looking, active array antenna (0.5m by 2.0m) without obstruction [50]. Following subsections are the explanation of some SAR systems listed in Table 5.1.

5.2.1 E-SAR P-Band System

E-SAR is a multi-frequency SAR system which is owned and operated by DLR. It was mounted on board a Dornier DO-228 aircraft [51]. With the selection of vertical and horizontal antenna polarization, currently the radar is operational in P-, C-, L-, and X-Bands. Functional modes of radar are SAR interferometry and SAR polarimetry established in 1996 [52]. The resolution of E-SAR products is up to 1.5 m in slant range. The scene length is not limited in general where the typical swath widths are 3 and 5 km. Dornier 228 aircraft is equipped with a CCNS4/ Aerocontrol navigation system coupled with DGPS and INS for motion compensation which is an essential requirement for the generation of SAR images. This assures measurement of the platform position with accuracy of 0.1m rms and of its altitude by 0.01 degrees. The system also consists of new high power amplifier (HPA) of 53 dB gain and peak power of 200 Watts. To avoid signal distortion by out-of-band broadcasting frequencies additionally a 60MHz band-pass filter was implemented before the low noise amplifier. A new 50 dB PIN switch was implemented to achieve the high isolation requirements between the four polarization channels. Antenna which consists of a 2mx4m microstrip element array at a center frequency of 450 MHz is the core elements for determining the system performance. The basic operating parameters of the E-SAR P-Band system are shown in Table 5.2 [53].

E-SAR P-Band System	
Parameter	Typical value
Center Frequency (MHz)	450
Pulse bandwidth (MHz)	18 or 50
Chirp duration (micro-sec)	5
Sample rate (MHz)	60
Forward velocity (m/s)	80-95
PRF (Hz/Channel)	500
Flight Altitude (m)	3000-5000
Incident angle (deg)	25-60
Interferometric mode	Repeat-Pass
Across-track baseline (m)	variable
Baseline tilt. Vert. (deg)	variable

Table 5.2: Basic operating parameters of the E-SAR P-Band system

5.2.2 EADS SAR

The first generation of the EADS SAR sensor system MISAR was introduced in 2003. MISAR is a much miniaturized Ka-band FMCW (Frequency Modulated Continuous Wave) SAR sensor. It was designed for small UAVs with a payload allowance of less than 5 kg. The very first flight-test of a SAR system onboard a mini-UAV was conducted with this sensor. High-quality imaging from such small platforms could successfully be demonstrated. Numerous flight tests followed and the experience obtained in these experiments lead to the development of the second-generation MISAR. The main improvements in the fields of image processing, MTI processing and ground segment MMI were described in the second generation MISAR [54].

5.2.3 RAMSES Airborne SAR

The airborne SAR Ramses was developed by French organization ONERA. It was flying onboard a Transall C160 aircraft. Ramses is a multi-frequency and high resolution airborne SAR which use P-band since the end of 2000. The

operating frequency of P-band is 435 MHz using a 1.3 x 0.8 m patch antenna which is full polarimetric with an incidence angle ranging from 40 to 80 degrees. A range resolution of 3.5 m is due to high bandwidth of 70 MHz and the emitted power is more than 500 W. Direct chirp, deramping chirp, step frequency are the several available operation modes and onboard calibration is performed [55]. These types of P and L band SAR systems are usually utilized for earth observation and remote sensing applications.

5.2.4 PHARUS - TNO-FEL

PHARUS (Phased Array Universal SAR) was developed by the TNO Physics and Electronics Laboratory (TNO-FEL), National Aerospace Laboratory (NLR) and the Delft University of Technology, Telecommunication and remote sensing Laboratory Netherland. It became possible after years of experience with real-aperture Side looking Airborne Radar (SLAR). PHARUS project consist of two phases, a definition phase and a realization phase. In definition phase knowledge about SAR was gained and critical information was gathered for final stage. Upon built up enough experience and completion of the preparatory studies, the system was realized in the period of 1991-1993. SAR testbed PHARS were designed to test modern technology of PHARUS. For transmission and reception a single antenna fixed to the aircraft was used in testbed. The antenna consisted of eight rows of four elements each. The four elements are connected by transmission lines and radiate equally to narrow the vertical antenna beamwidth to approximately 24 degree as desired. The eight radiating sections of the antenna were each connected to the T/R modules [56].

The eight modules were connected by a power splitter/combiner network with the frequency generator and detector which use a dielectric resonator oscillator (DRO) to generate microwave carrier. A single side band modulator with a digital generated linear FM chirp of 31 MHz bandwidth was used to modulate 5.3 GHz signal. Final PHARUS system use an increased bandwidth of approximately 100 MHz which necessitating a high IF frequency. Each transistor power amplifier on the PHARS delivers 20 Watts which resulting in total transmitted power of 160 Watts. In PHARUS system the pulse compression ratio has been further increased and the peak power increased to 2 kW approximately.

The digitizer and presummer of the PHARS also consisted of a monitor and AGC (Automatic Gain Control). After azimuth presumming the remaining digital data with a factor of 16 recorded on an airborne instrumentation recorder with HDDR. Aircraft altitude, antenna altitude and timing data were recorded besides the digital output of the digitizer and presummer. High exploitation cost of the system and the limited availability were the shortcomings. Afterall the testbed PHARS was not an operational system [56]. To address this need, a miniature, lightweight, low cost scalable SAR/MTI system called 'Mini-SAR' was developed by TNO.

5.2.5 Mini-SAR

In 2002 TNO-FEL developed a miniature, lightweight, low cost scalable SAR/MTI system called 'Mini-SAR'. It is designed for use in medium altitude UAVs and manned platforms with operating in X-band with a center frequency of 7.5 GHz. Its antenna panel length is 15 cm and total antenna length is 45 cm. The resolution of Mini-SAR was 30 cm or less and in high-resolution mode it will

cover at least 1 km swath, at about 3 km range. Moving target indication (MTI) mode of Mini-SAR can operate simultaneously with the typical SAR modes and detect slow moving targets at speeds greater than 3 km/h. Summary and system specifications of the Mini-SAR prototype are shown in Table 5.3 [57].

MiniSAR prototype System	
Parameter	**Typical value**
Weight	<50 kg (<30 kg design goal)
Power consumption	<1.5 kW (1 kW design goal)
Volume	To be fitted in COTS pod
Data storage	On-board
SAR mode	
Resolution	<0.5 m (0.3 m design goal)
Swath	>2 km (4 km design goal)
Frequency	X-band (10 GHz)
SAR Processing	Offline: Spotlight SAR mode
Range	>7km
Azimuth Resolution	0.05 m
MTI mode	
Number of channels	3
Minimum detectable velocity (MDV)	<10 km/h (5 km/h design goal)
Range	>10km

Table 5.3 Summary and system specifications of the Mini-SAR prototype

5.2.6 MicroSAR (μSAR)

A low-cost Micro Synthetic Aperture Radar (μSAR) was developed by Brigham Young University (BYU). The simple design based on a linear frequency modulated continuous wave signal (LFM-CW). It has compact size and less consumption of power as compared to a conventional pulsed SAR system. This enables the BYU μSAR to fly on a small unmanned aerial vehicle (UAV). Its low cost of operation extended its use into new areas. μSAR system consists of a stack of custom micro-strip circuit boards in order to minimize size, weight and cost of the

BYU μSAR. By using no enclosure the weight of the overall system is reduced further. Its weight is less than 2 kg in all, including antennas and cabling. Transmitter, Receiver, power, digital and A/D systems are five subsystem of the μSAR system architecture. Each subsystem is built upon its own customs board or shared between boards. Coaxial cables and wires are used for the interconnection of subsystems. The μSAR is designed for "turn-on and forget" operation. The system collects data continuously for up to an hour once powered up. For post-flight analysis the data are stored on the board. Simplified block diagram of μSAR is shown in Figure 5.1 [58].

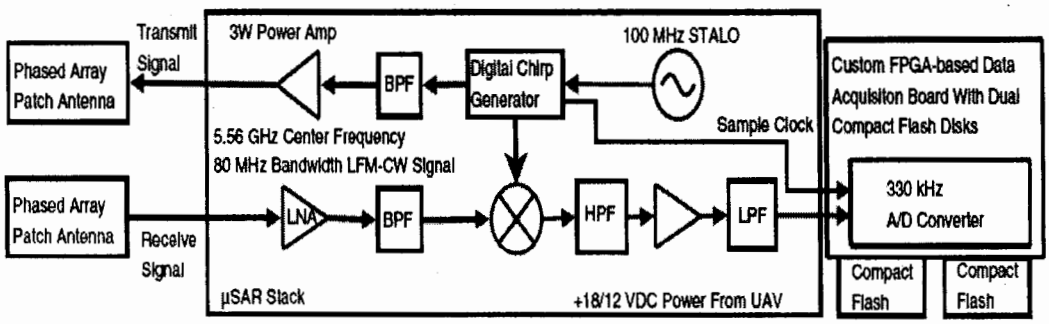

Figure 5.1: Simplified block diagram of μSAR

A 100 MHz stable local oscillator (STALO) is the core of the system. The frequencies for operating the system including the radar chirp and the sample clock are derived from this single source. Direct Digital synthesizer (DDS) is used to create LFM-CW transmit digitally which is controlled by a programmable IC microcontroller. By controlling the PRF setting by switches it is allowed to fly over different speed and heights. The sample clock coherent with the LFM signal is also generated by the programmable DDS.

The frequency of the LFM-CW signal is multiplied and the signal is amplified. Then it is split with one copy is being transmitted and the other copy of the signal is being mixed with the return signal. The LFM-CW signal is transmitted with

a power of 28 dBmW at a center frequency of 5.56 GHz and bandwidth of 80 MHz after amplification. The range resolution of an LFM chirp is inversely proportional to the bandwidth of the chirp. Thus μSAR has a range resolution of 1.875 m.

The returned signal is mixed with the transmitted signal after amplification. This de-chirped signal is sampled with a 16 bit A/D at 328.947 kHz after filtering. A custom FPGA board was designed to sample the signal and a pair of 1 GB Compact Flash disks is used to store the data. At a rate of 0.63 MB/second the data is collected continuously [58].

A center frequency 5.56 GHz was chosen by μSAR because it is in the unlicensed Wi-Fi band. Other devices can cause interference in the received signal, using frequencies within the bandwidth of μSAR. The effects can be reduced by filtering sections of higher than average power in the raw data [59].

5.2.7 Microsatellite circularly Polarized Synthetic Aperture Radar (μ SAT CP-SAR)

Recently the developing of the circularly Polarized Synthetic Aperture Radar (CP-SAR) onboard microsatellite (μ SAT CP-SAR) was in process in Japan. Until now all SAR sensor used linear polarization. The purpose of CP-SAR is especially to the monitor global vegetation, cryosphere and disaster area in the future and also to retrieve the physical information of the Earth surface. Circularly polarized wave is used for transmission and reception in CP-SAR. It is a low cost, light, low power, simple, strong and low profile configuration which uses right-handed circular polarization (RHCP) for transmission (Tx) and left-handed circular polarization (LHCP) +RHCP for reception (Rx). Axial ratio image (ARI) is generated by these

circularly polarized waves. Due to eliminating effect of Faraday rotation during the propagation in ionosphere, CP-SAR is expected to produce a high precision and low noise image. This satellite planned to be launched in 2014 with altitude between 500 km and 700 km. Chirp pulse bandwidth of 10 MHz and center frequency on L band (1.27 GHz) is used for operation of this sensor. To obtain ideal circular polarization the axial ratio is set lower than 3 dB. The antenna size is 4m and 8m for range and azimuth directions, respectively. The swap width is 50 km and center of off-nadir angle is set to 29 degree. Specifications of CP-SAR onboard microsatellite is shown in Table 5.4 [60].

Microsatellite CP-SAR System	
Parameter	**Specification**
Altitude	500 km ~ 700 km
Inclination angle	98 degrees
Frequency	1.27 GHz (L-Band)
Chirp Bandwidth	10 MHz
Polarization	Transmitter: RHCP
	Receiver: RHCP + LHCP
Gain	>30 dBi
Axial ratio	<3 dB (main beam)
Antenna size	8 m (azimuth)
	4 m (range)
Ground resolution	15 m
Swath width	50 km
Off nadir angle	29 degree
PRF	2000 ~ 2500 Hz
Power	90 W
Size	50cm x 50cm x 70cm
weight	<100 kg

Table 5.4: Specifications of CP-SAR onboard microsatellite

CHAPTER 6 THEORY OF SIMULATION

In this chapter we will present the theory of processing techniques used in the Simulation of SAR image and the results are given in chapter-7. Processing techniques involved Matched Filtering and Doppler beam Sharpening algorithm. Other terms Doppler Frequency, Linear modulated Chirp signal and Pulse related to simulation radar are also discussed.

6.1 Sidelobe Suppression by windowing function

The most common sidelobe suppression technique is to apply a window function. In FIR filter design, we apply the window to the filter impulse response in the time domain in order to reduce the filter sidelobes (stopband response) in the frequency domain. That is, if we want to suppress sidelobes in one domain, we apply the window in its complementary Fourier domain. Applying this thinking to the LFM matched filter, we want to suppress sidelobes in the time (range) domain; therefore we should apply the window in the frequency domain.

One way to do this would be to perform conventional matched filtering in the fast time domain; compute the DFT of the matched filter output; apply the window to that spectrum; and then take the inverse DFT to obtain the reduced-sidelobe response. However, by performing the matched filtering in the frequency domain, we can combine the matched filter operation with the windowing to reduce the required computation. A block diagram of one way to arrange the flow of operations is shown in Figure 6.1. This diagram shows the window applied to the filter frequency response before the actual filtering step. This has the advantage of allowing the windowing to be done off-line, *i.e.* not in real time. We could just as

well apply the window to the product of the signal and matched filter frequency responses. The end result at the output would be identical, but the windowing would have to be repeated every time there was a new signal to filter, and in real time [66].

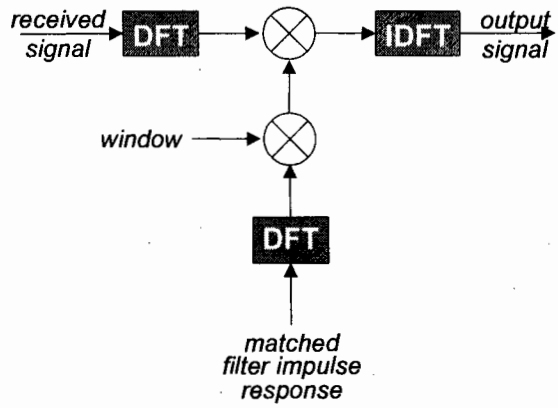

Figure 6.1: Flow diagram for LFM sidelobe suppression by frequency domain windowing.

6.2 Matched Filter

A matched filter (receiving network) maximizes the ratio of peak signal power to average noise power for an instant in time. If the signal changes the filter must change so it is matched to the signal being used. A matched filter is designed to provide maximum signal to noise ratio at its output for a transmitted signal [62].

If $f(t) \leftrightarrow F(\omega)$ is the frequency response of the input signal, than a network of frequency response $h(t) \leftrightarrow H(\omega)$ is matched to the input signal if $H(\omega) = F^*(\omega)$ or $\{h(t) = f(-t)\}$. In the presence of white noise it will maximize the peak output signal voltage to rms out put noise voltage that is 2E / No. Therefore the maximum signal to noise ratio will depend on the input signal energy and the power spectral density of the noise rather than the particular shape of the waveform used. The

impulse response of the matched filter is $h(t) \leftrightarrow F^*(\omega)$ or $h(t) = f(-t)$ i.e. h(t) is the time reverse of the matched input signal f(t). The output of matched filter g(t) will be :

$$g(t)=f(t)*h(t) = f(t)*f(-t)= \int f(x)f(x-t)dx \qquad (6.1)$$

Hence the equation depicts the auto correlation function of f(t) [63]. The term-matched filter is often used synonymously with product integrator or correlator. However, it must be understood that the correlator output and the matched filter output are equal only at sampling instant (t = T) as shown below.

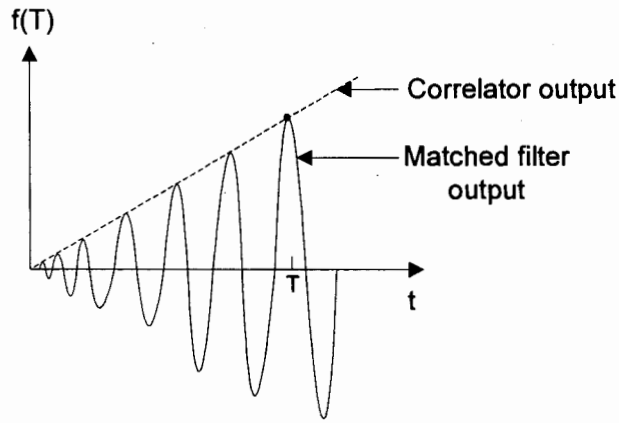

Figure 6.2: Comparison of Matched Filter and Correlator

It can be summarized that the basic characteristics of the matched filter is that its impulse response is a delayed version of the mirror image (rotated on the t=0 axis) of the input signal waveform.

6.3 FM Chirp Signal

For good detection in radar environment long duration pulse are required in order to increase signal energy [64]. However, to improve target resolution (a term used to imply that two or more targets are separated to perform necessary measurements) short duration pulses are required. With the help of FM a waveform can be designed to have both long duration and small effective duration (large

bandwidth). This can be achieved in conjunction with a matched filter and the signal processing technique is called pulse compression. The linear FM pulse is called chirp signal and can be represented by the following simplified equation for a linear increase of frequency with time: -

$$f(t) = \cos(\omega ot + \pi F/T\, t^2) \quad \text{for} \quad -T/2 < t < T/2 \tag{6.2}$$

Where $F = f_2 - f_1$ is the sweep bandwidth with f_1 and f_2 being the initial and final instantaneous frequencies and T is the duration as depicted in Figure 6.3.

Linear frequency modulation (LFM) pulsed signals (usually called chirp signal) are preferred transmitted signals used to obtain wide frequency band within a relatively wide time width. By using chirp signals high peak power can be avoided and hence reducing complexity of the radar system.

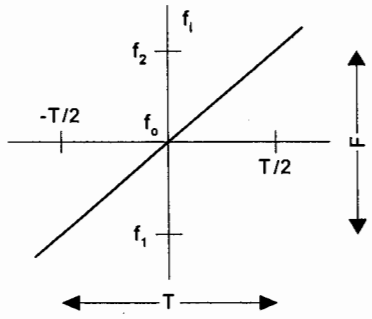

Figure 6.3: Chirp Signal

6.4 Doppler Beam Sharpening (DBS) Algorithm

Doppler Beam Sharpening commonly refers to the method of processing unfocused real-beam phase history to achieve better resolution than could be achieved by processing the real beam without it. Because the real aperture of the RADAR antenna is so small (compared to the wavelength in use), the RADAR energy spreads over a wide area (usually many degrees wide in a direction orthogonal (at

right angles) to the direction of the platform (aircraft). Doppler-beam sharpening takes advantage of the motion of the platform in that targets ahead of the platform return a Doppler upshifted signal (slightly higher in frequency) and targets behind the platform return a Doppler downshifted signal (slightly lower in frequency).

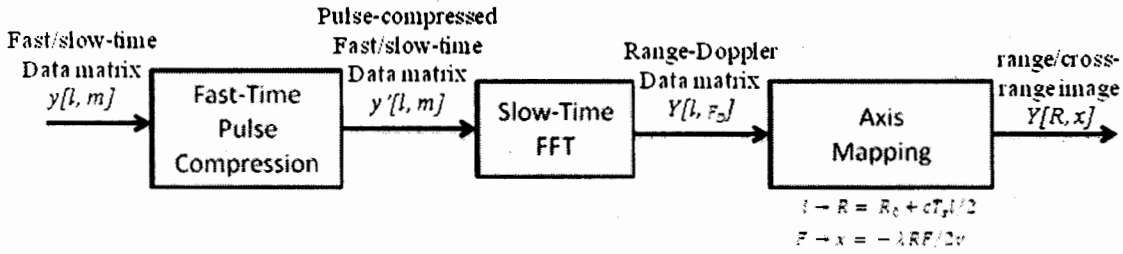

Figure 6.4: Block diagram of DBS algorithm

The amount of shift varies with the angle forward or backward from the ortho-normal direction. By knowing the speed of the platform, target signal return is placed in a specific angle "bin" that changes over time. Signals are integrated over time and thus the RADAR "beam" is synthetically reduced to a much smaller aperture – or more accurately (and based on the ability to distinguish smaller Doppler shifts) the system can have hundreds of very "tight" beams concurrently. This technique dramatically improves angular resolution; however, it is far more difficult to take advantage of this technique for range resolution [65].

This algorithm is the original form of SAR envisioned. For all ranges a constant aperture time is used in DBS. It has relatively low computational requirements and provides a substantial improvement over real beam cross-range resolution. To get desired cross-range resolution data is collected over selected aperture time Ta. Doppler spectrum is computed in each range bin using Discrete Fourier Transform (DFT) to produce range-Doppler image. Block diagram of DBS algorithm is shown in Figure 6.4 [66].

6.5 Pulse Doppler radar

Pulse Doppler is a radar system capable of not only detecting target location (bearing, range, and altitude), but also measuring its radial velocity (range-rate). It uses the Doppler Effect to determine the relative velocity of objects; pulses of RF energy returning from the target are processed to measure the frequency shift between carrier cycles in each pulse and the original transmitted frequency. To achieve this, the transmitter frequency source must have very good phase stability and the system is said to be coherent [65].

The nature of pulsed radar, and the relationship between the carrier frequency and the pulse repetition frequency (PRF) means that the frequency spectrum can be very complex, leading to the possibility of errors and tradeoffs. In general, it is necessary to utilize a very high PRF to avoid aliasing, which can cause side effects such as range ambiguity. To avoid this, multiple PRFs are often used [65].

6.6 Characteristics of the Target

When a signal impinges upon a target it is reflected in various directions. The nature of reflections depends on the behavior and characteristics of the target. The Radar Cross Section (RCS) of a reflecting object is defined as the ratio of power density of the signal reflected in the direction of the receiver to the power density of the radio wave incident upon the target. Thus Radar Cross Section is the measure of target's ability to reflect radar signals in the direction of receiver. The units of RCS are square meters and measurements for the signal reflected from the target are made in comparison to the signal reflected from a perfectly smooth sphere having cross sectional area of one m^2.

CHAPTER 7 SIMULATIONS RESULTS

MATLAB and Simulink tools are used for simulation of different features of SAR i.e. is Characteristic of Linear Frequency Modulated (LFM) pulse, Pulse Compression of LFM, Pulse Doppler Radar and Doppler Beam Sharpening (DBS) algorithm for simulation of range and cross-range image of SAR.

7.1 Characteristic of Linear Frequency Modulated (LFM) Pulse

MATLAB is used to study the various characteristic of LFM pulse by using different bandwidths, and applying matched filtering for comparison of simple and LFM pulse. To decouple waveform energy and improve range resolution a LFM modulation technique is used. Much wider operating bandwidths can be achieved by using Frequency or phase modulated waveforms. Linear Frequency Modulation (LFM) is commonly used to improve target resolution. In this case, the frequency is swept linearly across the pulse width, either upward (up-chirp) or downward (down-chirp). The matched filter bandwidth is proportional to the sweep bandwidth, and is independent of the pulse width.

7.1.1 Effects of BT Product on Chirp Spectrum

Effects of Bandwidth Time (BT) product on chirp Spectrum is shown in the Figure 7.1. In this Figure three chirp pulses were generated of same pulse duration of 100e-6 seconds but with swept bandwidths of 100 KHz, 1 MHz and 10 MHz at an over sampling factor of k=1.2. All the three spectra have the same bandwidth in the plot as the frequency is normalized. The amplitudes of the spectra differed significantly. The spectrum amplitude is proportional to bandwidth. As bandwidth increased spectrum amplitude also increased. It is proved that sampling

rate also increases with increase in bandwidth. Since the chirp bandwidths differ, the sampling rate T_i for each chirp is different.

$$F_{s_i} = k\beta_i \quad \Rightarrow \quad T_i = \frac{1}{k\beta_i}$$

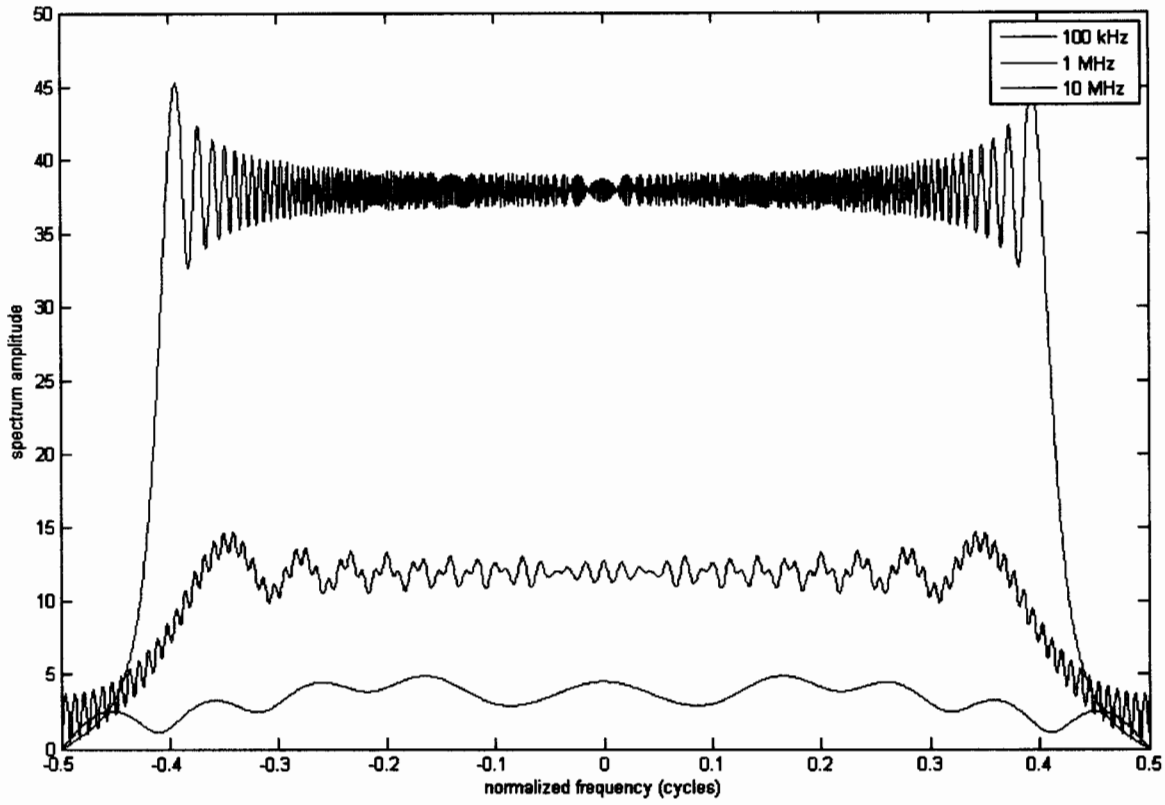

Figure 7.1: Three LFM Pulses with different BT Products

Since each pulse shares duration of 100 *m*s, this also means that the number of samples in each pulse is different and in fact is proportional to the bandwidth:

$$N_i = \frac{\tau}{T_i} = \tau F_{s_i} = k\tau\beta_i$$

It can be said that by increasing bandwidth time product we can approximate magnitude of Fourier transform of a chirp with a rectangle function.

7.1.2 Comparison of Simple and LFM pulse by Matched Filtering

Comparison of Simple pulse and LFM pulse is shown in Figure 7.2 after Matched Filtering. A simple pulse & LFM pulse of kxτpxb =10x100e-6x1e6 samples were generated. Same peak magnitudes were observed at matched filter output of both simple and LFM pulse. As same peaks were observed for both the simple and LFM pulse therefore the two waveforms have same energy. LFM decouple energy and pulse while Simple Pulse coupled energy and pulse. Matched filter output of simple pulse is a triangle and is shown in Figure 7.2 while matched filter output of a LFM is a narrow Sinc pulse. Simple pulse gives coarse resolution

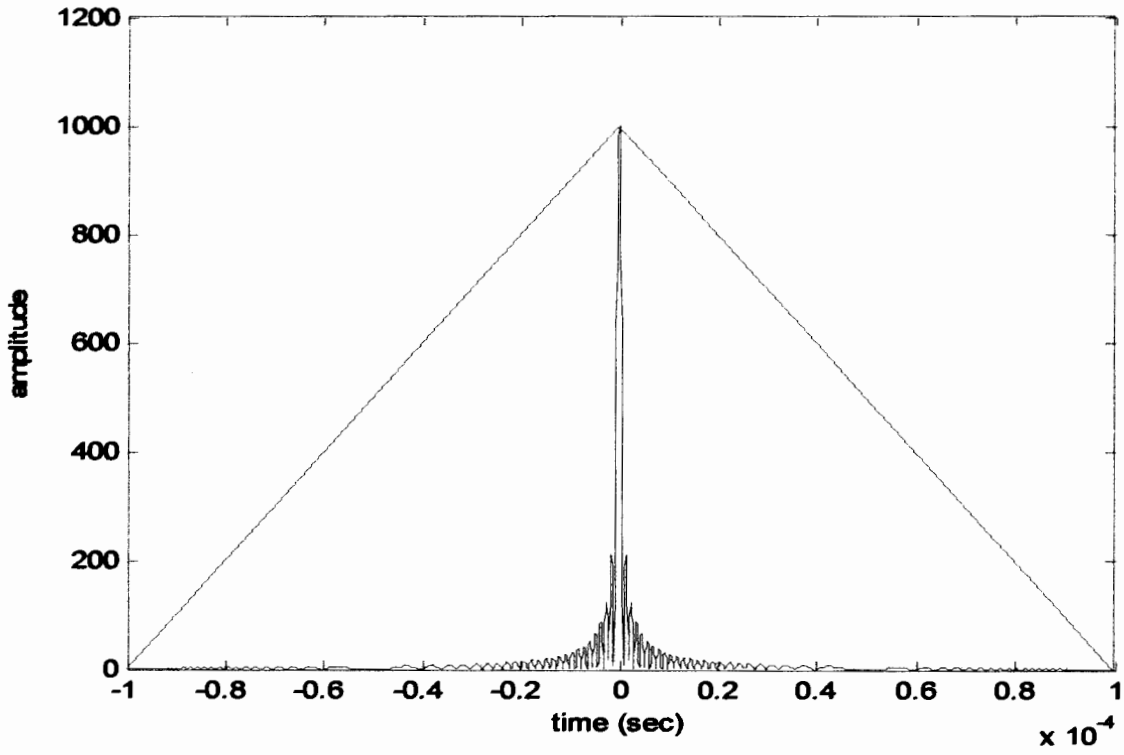

while LFM gives finer resolution.

Figure 7.2: Matched Filter output of LFM pulse and Simple Pulse

The LFM chirp is called a "pulse compression" waveform because most of its energy at the output of the matched filter is compressed into a much narrower spike than is the case for the simple pulse of the same length.

7.1.3 Resolution Comparison of LFM and Simple Pulse

To confirm the higher range resolution of the LFM chirp, we consider two scatterers 10 microseconds apart in received echo time corresponding to (c/2)x10 ms = (3e8 x 10e-6)/2=1500m= 1.5 km of range separation. A simple pulse & LFM pulse of k x τ x b =10x10e-6x1000000(Hz) = 100 samples were generated. Thus, our respective received signals are created by simply overlapping copies of the transmitted pulse, separated by 100 samples, for each of the two pulse types of interest. We then matched filter the two sequences. The results are shown in Figure 7.3.

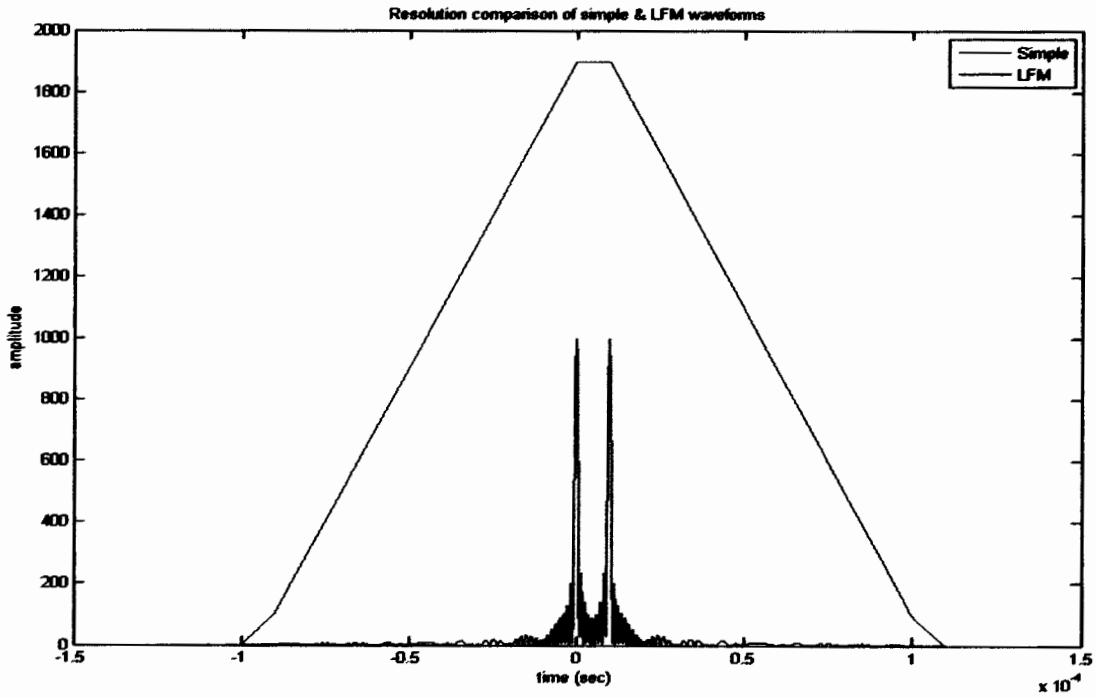

Figure 7.3: Resolution comparison of simple & LFM pulse

The simple pulse completely fails to resolve the two targets, while the LFM chirp resolves them easily, meaning that two distinct and easily separable peaks are visible at the matched filter output.

7.1.4 Range-Doppler Coupling

We expect the Doppler shift to cause the peak of the matched filter output response to be shifted away from its correct location. Doppler shift corresponding to 10% of the swept bandwidth (thus, 100 kHz) imposed on the returned echo. The predicted shift in the peak location is

$$\Delta t_{peak} = -\frac{F_D \tau}{\beta} \quad \text{seconds}$$

$$= -\left(\frac{\beta}{10}\right)\frac{\tau}{\beta} = -\frac{\tau}{10} = -10\mu s$$

where we have used the particular values τ = 100 μs in the last step of the equation above. We thus expect the matched filter output peak to occur 10 μs early.

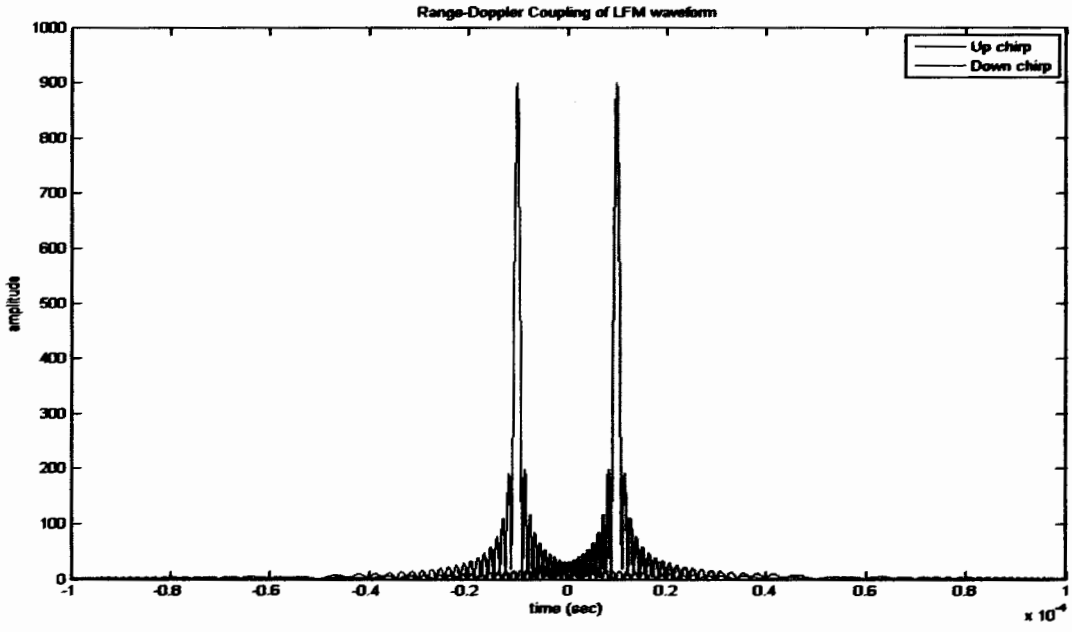

Figure 7.4: Range-Doppler coupling of LFM waveform

The leftmost peak in Figure 7.4 is the response of the matched filter for the up chirp waveform and the specified Doppler shift. The peak occurs at -10 μs as predicted.

The second (rightmost) peak in Figure 7.4 is the result when we use a down chirp with the same swept bandwidth and duration as the original up chirp; we simply reverse the direction of the frequency sweep. The same positive Doppler shift is applied to the waveform, and the peak now occurs at $+10$ μs.

At least for isolated (separated) targets, we could transmit an up chirp on one pulse, and the corresponding down chirp on the next pulse. The true range location would then be the average of the two measured peak locations, since they will be displaced from the correct location by equal amounts but in opposite directions.

We should expect a reduction in peak amplitude as the filter is no longer matched to the received waveform (due to the extra Doppler term). In fact, we can see that the peak is reduced from a value of 1000 in figure 7.1 to 900 in Figure 7.4.

7.2 Sidelobe Suppression

We can see from observation of Figure 7.2 that the peak sidelobe in the LFM matched filter output is approximately 13.4 dB below the peak. This should not be surprising; the spectrum is, by design, approximately a rectangle function so that its inverse Fourier transform is approximately a sinc function, which would have -13.2 dB peak sidelobes. On the other hand, the spectrum is not an exact rectangle, so

we do not expect exactly –13.2 dB peak sidelobes. In many applications -13 dB sidelobes are not acceptable and must be reduced.

Figure 7.5 illustrates the application of a Hamming window function to the LFM chirp oversampled by 1.2. The DFT of the chirp has been rotated to place the zero frequency point in the middle of the plot. Note that the window function should be has been aligned so that its center is aligned with the center of the LFM spectrum. Furthermore, the width of the window corresponds to the nominal width of the LFM spectrum, namely $\pm\beta/2$ Hz.

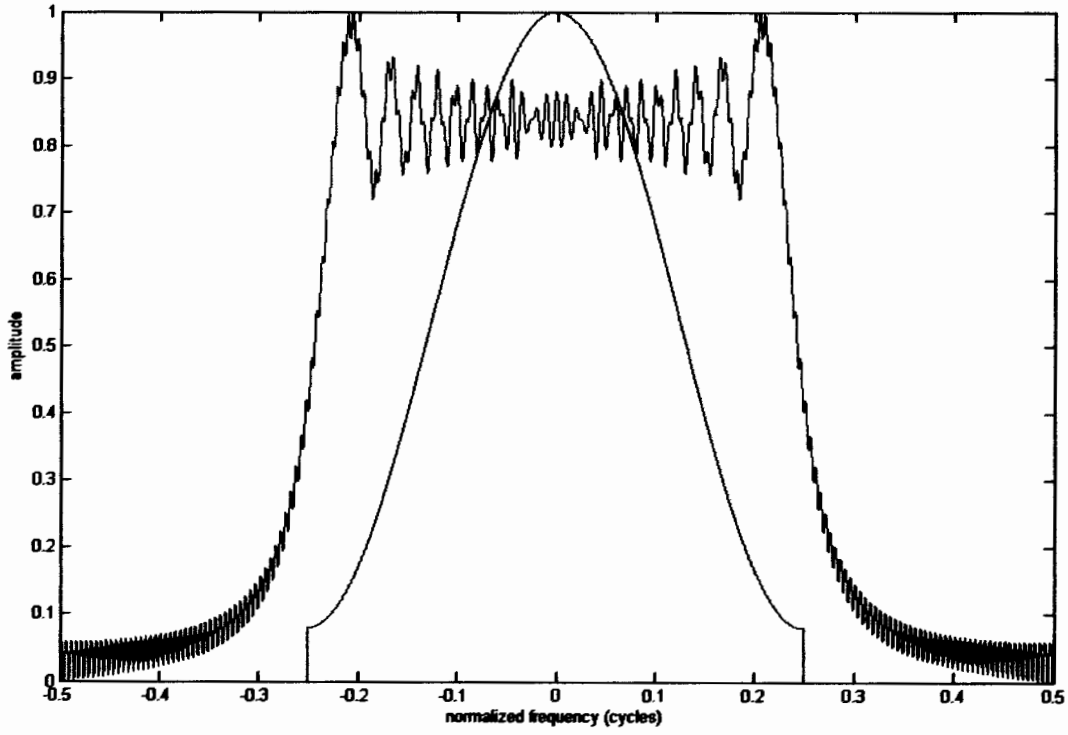

Figure 7.5: Hamming window function aligned with respect to chirp spectrum and cut off at $\pm\beta/2$ Hz.

Figure 7.6 shows the output obtained by applying the operations shown in Figure 6.1 to the echo from a single point scatterer, that is, to a replica of the

transmitted waveform. An oversampling rate of 10 was used. The results are shown with and without Hamming weighting.

The windowed filter response suffers a loss in the absolute response of the peak. This is inevitable because the window modifies the matched filter frequency response, so that it is no longer exactly matched to the transmitted waveform. Consequently, there must be a loss in peak response.

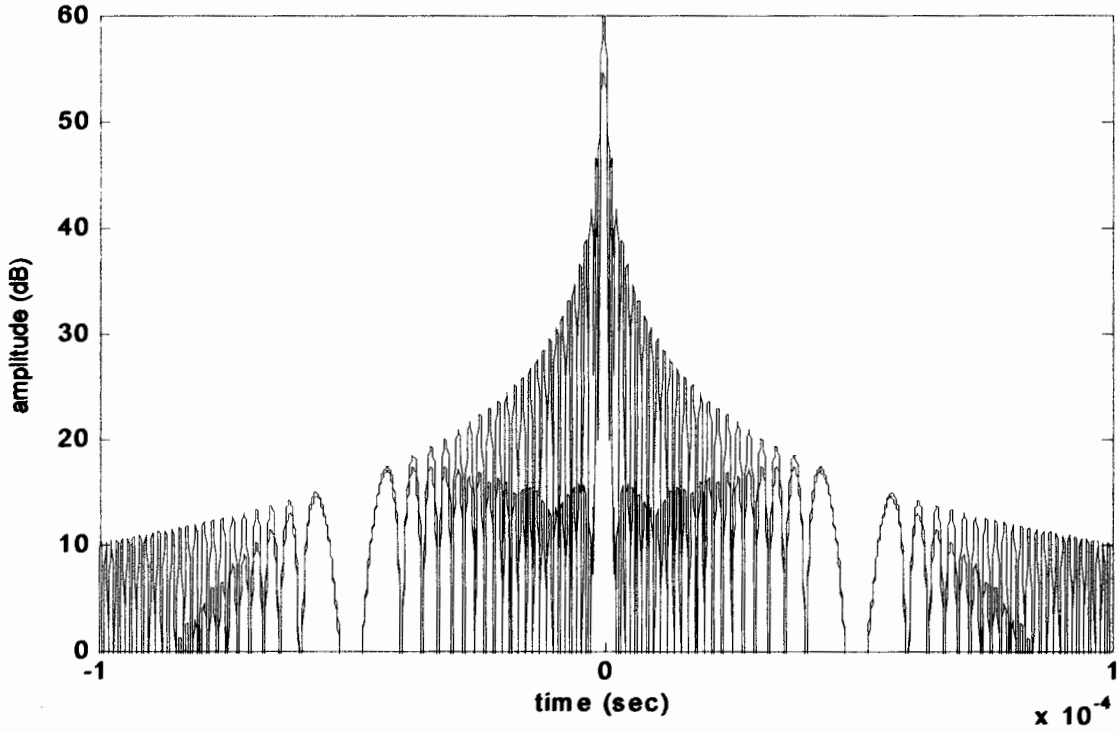

Figure 7.6: Output of frequency domain matched filter, with and without Hamming weighting.

In Figure 7.6 the peak is reduced from 60 dB to 54.65 dB, a loss of 5.35 dB. The predicted loss is given by

$$LPG = \frac{1}{K^2}\left|\sum_{k=0}^{K-1} w[k]\right|^2$$

A 16,384 point FFT was used for the DFTs in my solution to get good detail in the spectrum. The size of the Hamming window is then (16,384/10), which rounds to 1,638 samples. Evaluating the equation for LPG for a 1638-point Hamming window gives a predicted loss of 5.36 dB, in excellent agreement with the measured value of 5.35 dB.

The primary purpose of windowing is reduction of sidelobes. The first sidelobe is 13.5 dB below the peak for the unwindowed case, and 41 dB below the peak for the windowed case. The peak sidelobe (not the same as the first sidelobe in the weighted case) is 37.2 dB down with weighting. Thus, use of the Hamming weighting has improved peak sidelobe suppression by 23.7 dB (37.2 – 13.5).

The final effect of interest caused by the windowing is the broadening of the matched filter mainlobe, which represents a loss of range (time) resolution. Inspection of the location of the first zero of the response for each case shows it to occur at about 1 μs in the unwindowed case, and 1.93 μs in the windowed case. This latter value is a little less than the 2 μs we would normally anticipate due to the 2x broadening expected of a Hamming window.

There is a legitimate question as to whether the Hamming window should be chosen to cut off at $\pm\beta/2$ Hz as shown in Figure 7.5. This choice is obviously motivated by the swept instantaneous frequency range of the chirp, but because of the modest BT product of 100, the spectrum does not cut off sharply at $\pm\beta/2$. Some perhaps non-trivial energy outside of $\pm\beta/2$ is zeroed by the window in this case. Figure 7.7 repeats the experiment of Figure 7.6, but with the Hamming window expanded by 10% in frequency to cover more of the LFM spectrum tails.

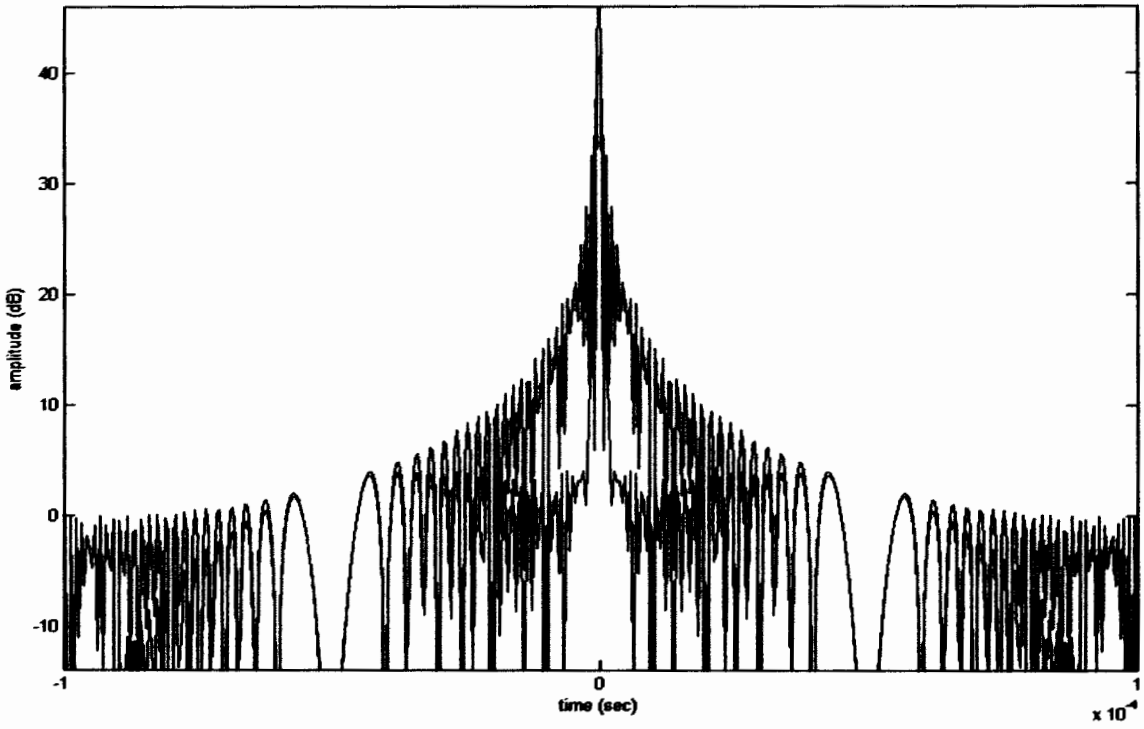

Figure7.7: Same as Figure 7.6, but with 10% expanded bandwidth Hamming window.

Close inspection of Figure 7.7 shows that the peak is now reduced only to about 55.4 dB. The corresponding loss is 4.6 dB instead of the previous 5.35 dB. Thus, the loss has been reduced (improved) by 1.34 dB by not discarding the energy at the tails of the spectrum. On the other hand, the peak sidelobe (which is now also the first sidelobe) is about 32.5 dB down from the peak, not quite as good as the 37.2 dB for the case where the Hamming window cutoff was at $\pm\beta/2$. As the BT product gets larger, the cutoff of the signal spectrum becomes sharper, so that for large BT products, one should most likely cutoff the window at $\pm\beta/2$ Hz.

Finally, we try time-domain weighting of the receiver impulse response. Using the principle of stationary phase, that an LFM pulse with a time-domain amplitude $A(t)$ would have a spectrum whose magnitude followed the same shape as $A(t)$, but spread over the frequency range $\pm\beta/2$ Hz. Since our goal is to achieve a filter impulse response whose spectrum has a Hamming shape, this means that applying the Hamming weight to the filter impulse response should achieve that result. The output of the resulting filter, shown in Figure 7.8, has the same general character as the frequency-domain weighting result of Figure 7.6, but with some differences in details of the sidelobe structure.

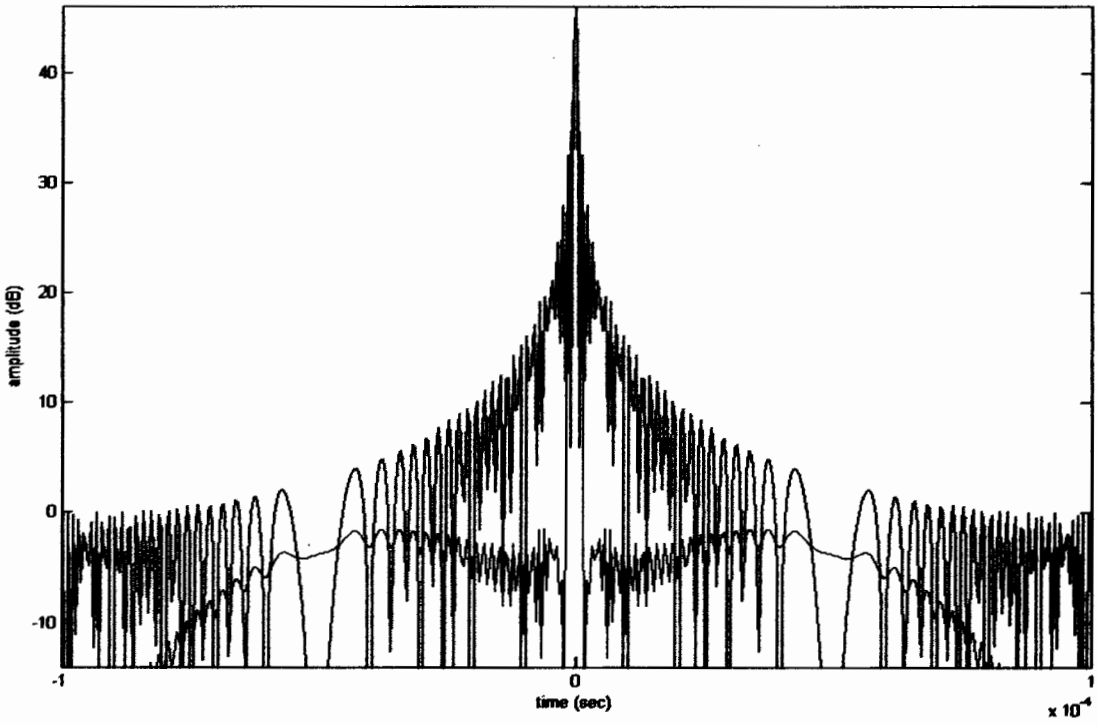

Figure 7.8: Matched filter output with and without time-domain weighting of the filter impulse response. Compare to Figure 7.6

The peak is reduced from 60 dB to 54.64 dB with weighting, a reduction of 5.36 dB that agrees with the predicted value. The peak sidelobe of the weighted response (which is the first sidelobe in this case) is 40.7 dB below the

mainlobe peak, 3.5 dB better than my first frequency-domain case. The Rayleigh width of the unwindowed case remains 1 μs, while the windowed case Rayleigh width is 1.97 μs; closer to the 2 μs expected for the Rayleigh window than the 1.93 μs we observed in the frequency domain weighted case.

7.3 Simulation of Pulse Doppler radar

Pulse Doppler radar has capability of detecting moving targets and measures its speed and direction. For simulation of Pulse Doppler radar we use MATLAB and SIMULINK. The system consists of SIMULINK models of the transmitter model, model of the target and model of signal processing end.

7.3.1 Overall System

The SIMULINK model of overall system is shown above in the Figure 7.9.

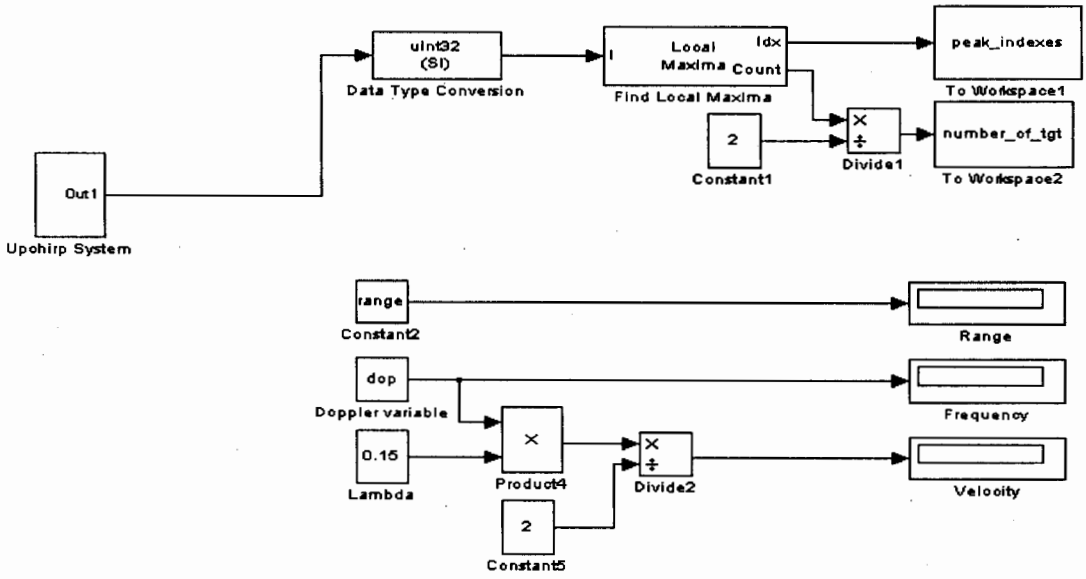

Figure 7.9: Overall System

Some important parameters of the model are Upchirp system block, finding local Maxima block, Range block, Frequency block and velocity block. The

"Upchirp System" block contains the transmitted waveform, the target model and the digital matched filter for the receiver. To find the number of peaks (targets) in the output we use "Find Local Maxima" block of the model. Radial distance is displayed by the "Range" block. "Frequency" block is used to find out Doppler shifts and the speed of the target is shown by "Velocity" block.

7.3.2 Pulse Transmitter Model

The Pulse Transmitter model is shown in Figure 7.10 which contains Pulse generator block, Upchirp block and the work space block. Pulse of finite duration and amplitude is generated by "Pulse generator" block. It provides a pulse train at its output. The "Upchirp" block provides a linearly swept sine wave at its output with a certain bandwidth, target time and sweep time. A copy of the transmitted signal is saved by the variable "Chirp_Template" in the workspace to be later used in the receive filter.

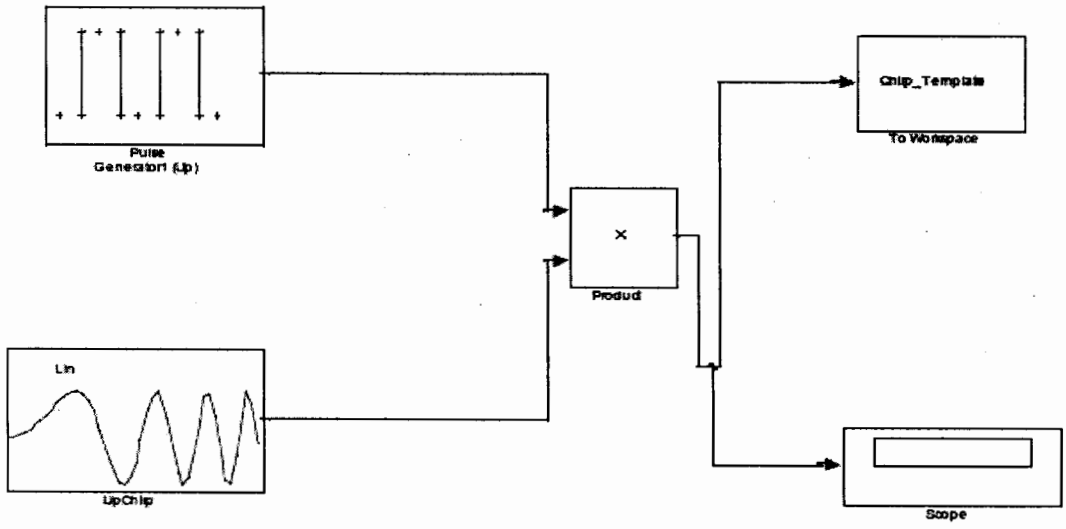

Figure 7.10: Pulse Transmitter model of radar system

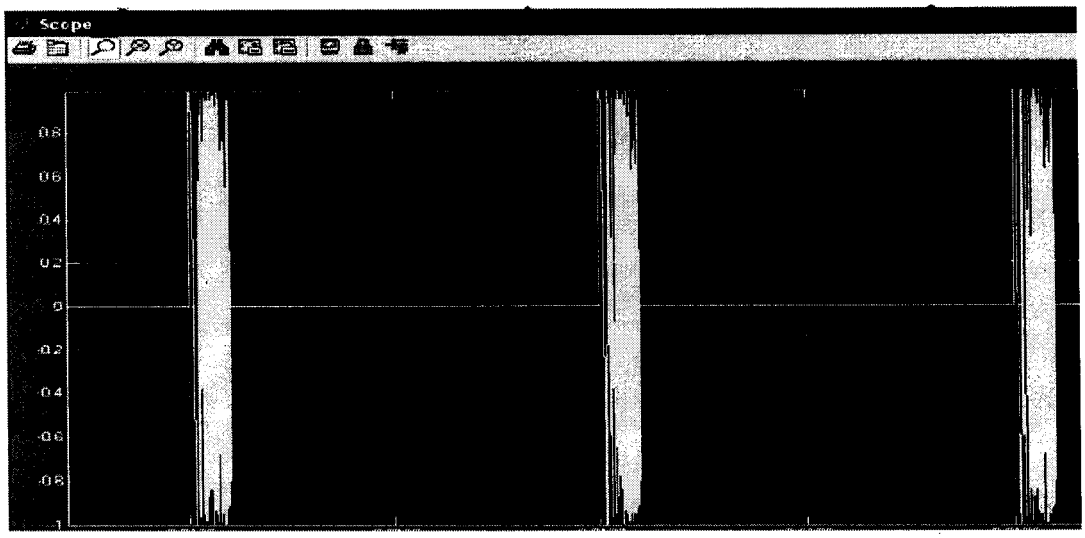

Figure 7.11: Transmitted LMF pulse (Time Domain Representation)

7.3.3 Target Model

Target model is shown in Figure 7.12 which consist of "Cosine Wave" block, "integer Delay" block, "Pulse generator" block, "Upchirp" block, "Scope" block "range equation" block and absolute value block. Functionality of Upchirp and pulse generator blocks is same as discussed above. The "Cosine Wave block" is used to provide a complex cosine wave which is used for the modeling of Doppler shift caused by a moving target. To model the delay in receiving, the return from a specific range "integer delay block" is used. "Range Equation" block is used to calculate the amplitude of the received signal. "Scope" block is used to represent the change in amplitude and frequency of the pulse return from the target.

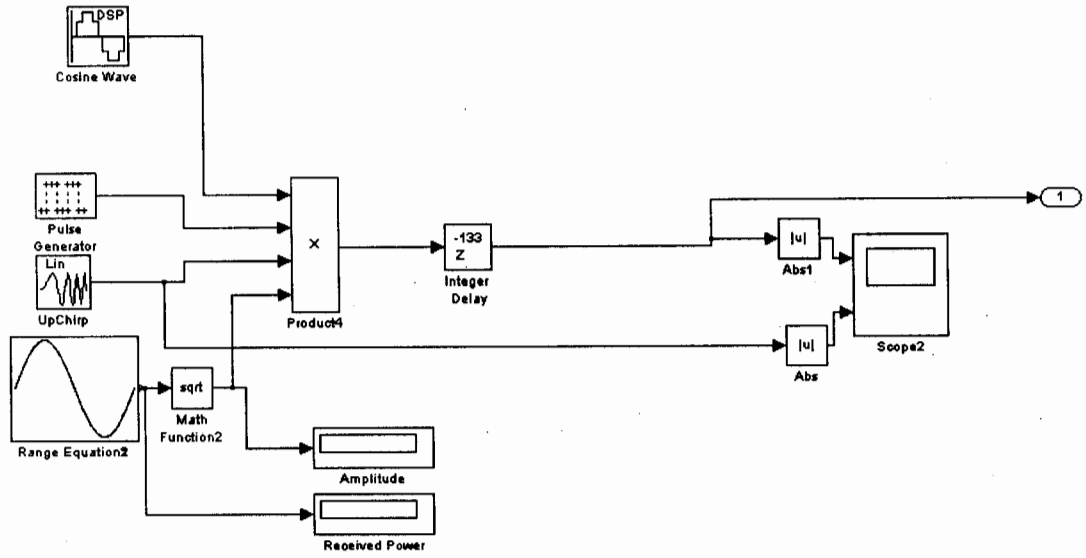

Figure 7.12: Target Model

We need to set the parameters of "integer delay" block according to our requirement, simply double click on it or use right click for properties and set it manually as shown in Figure 7.13.

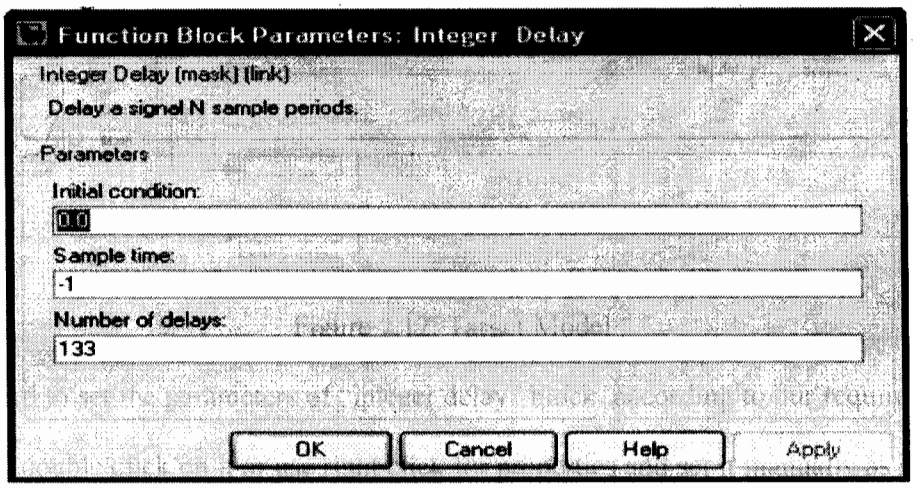

Figure 7.13: Setting the delay properties by target

Similarly we can set the parameters of "Range Equation" block. The variables involved in radar range equation are given to this block as input. The amplitude of the received signal is returned by this range equation block.

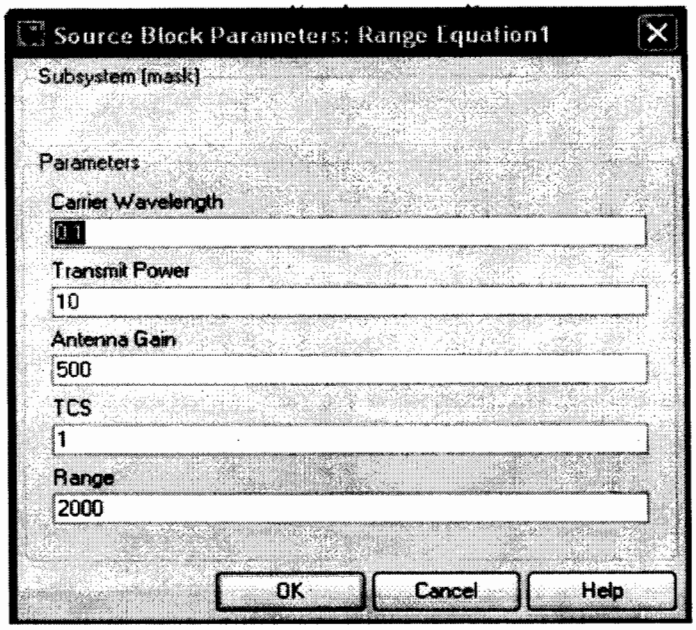

Figure 7.14: Setting the variable in range equation

Finally the "Scope" block shows the variation in the amplitude and frequency of the pulse returns from the target. We can view these variations by double clicking on Scope block.

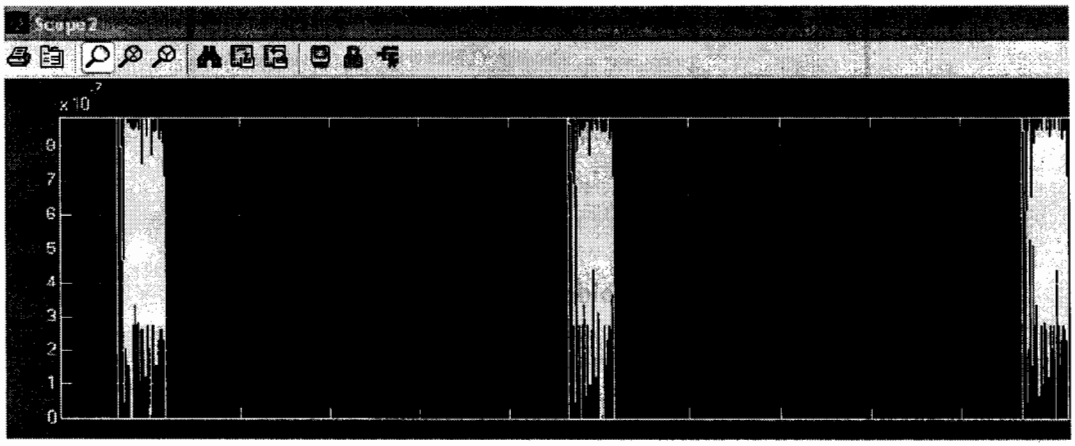

Figure 7.15: Returned waveform from the target

7.3.4 Signal Processor Model

Signal Processor Model is shown in the Figure 7.16. The return from the target is received by this model.

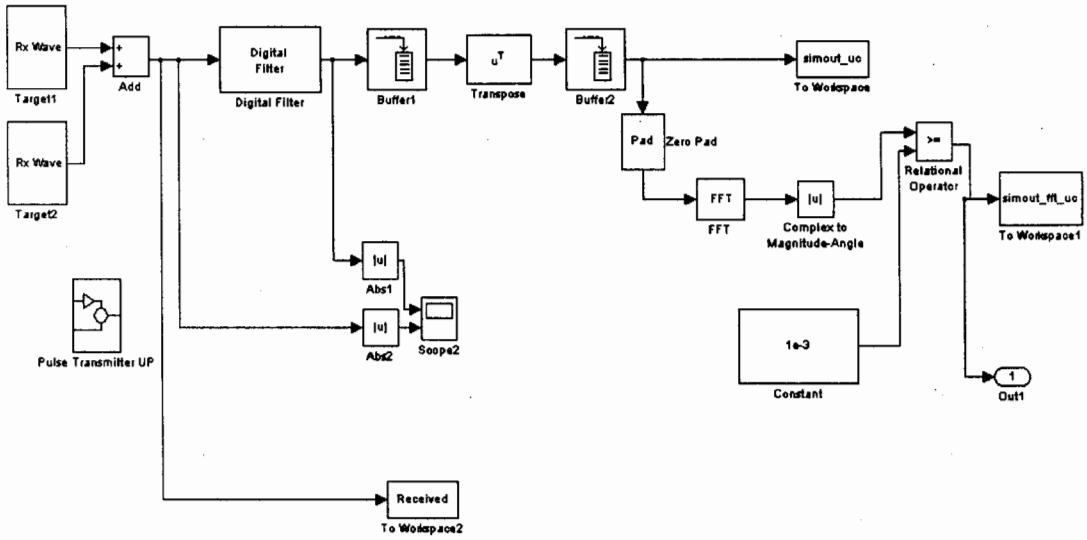

Figure 7.16: The Signal Processor Model

For pulse compression the received signal is then passed from the matched filter. To form a slow/fast time matrix, the buffers are used. Then Fast Fourier Transform (FFT) is applied on each column of the matrix. To decide about the presence of the target we use Threshold on the amplitude of the pulses. Workspace is used to store results. The inputs to the matched filter are shown in the lower half of the Figure and the compressed output of the matched filter is shown in the upper half.

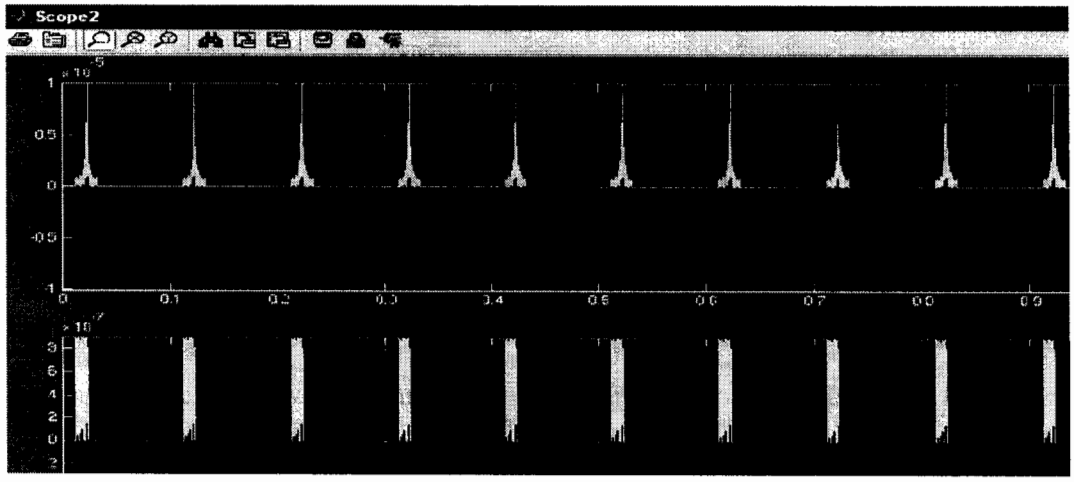

Figure 7.17: Inputs and Outputs of the receiver matched Filter

After simulating the overall system target model shown in Figure 7.9 we obtained the results of range Doppler shift as shown in Figure 7.18.

Simulation Parameters	
Range resolution	5 meters
Cross-range resolution	5 meters
Range to Central Reference Point (CRP)	40 km
Swath length	3000 m
Aperture time	0.8 seconds
Range curvature at CRP	0.045 meters
Pulse length	5 microseconds
Chirp bandwidth	30 MHz
Time-bandwidth product	150
Fast time sampling rate	60 Msamples/sec
PRF	3 kHz
PRI	333.333 usec.

7.4.1 Generated Raw Dataset

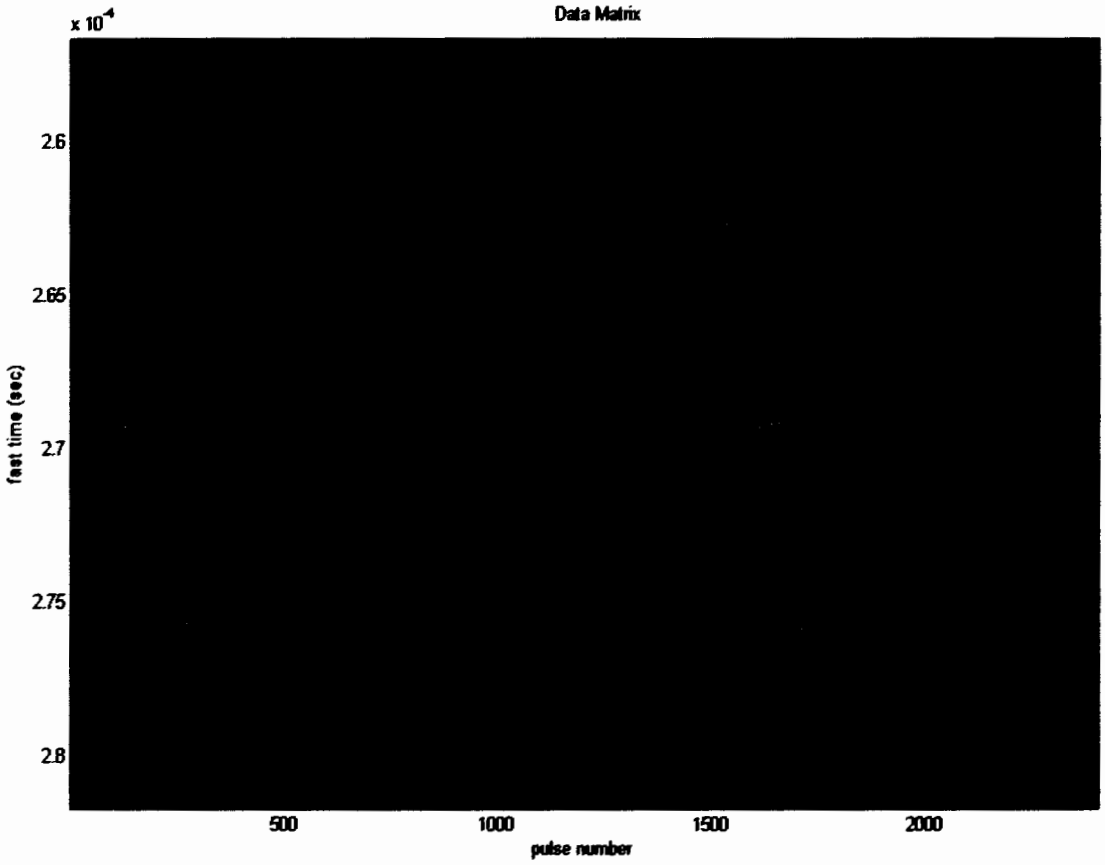

Figure 7.19: Generated Dataset for nine Scatteres

7.4.2 After Fast Time Pulse Compression

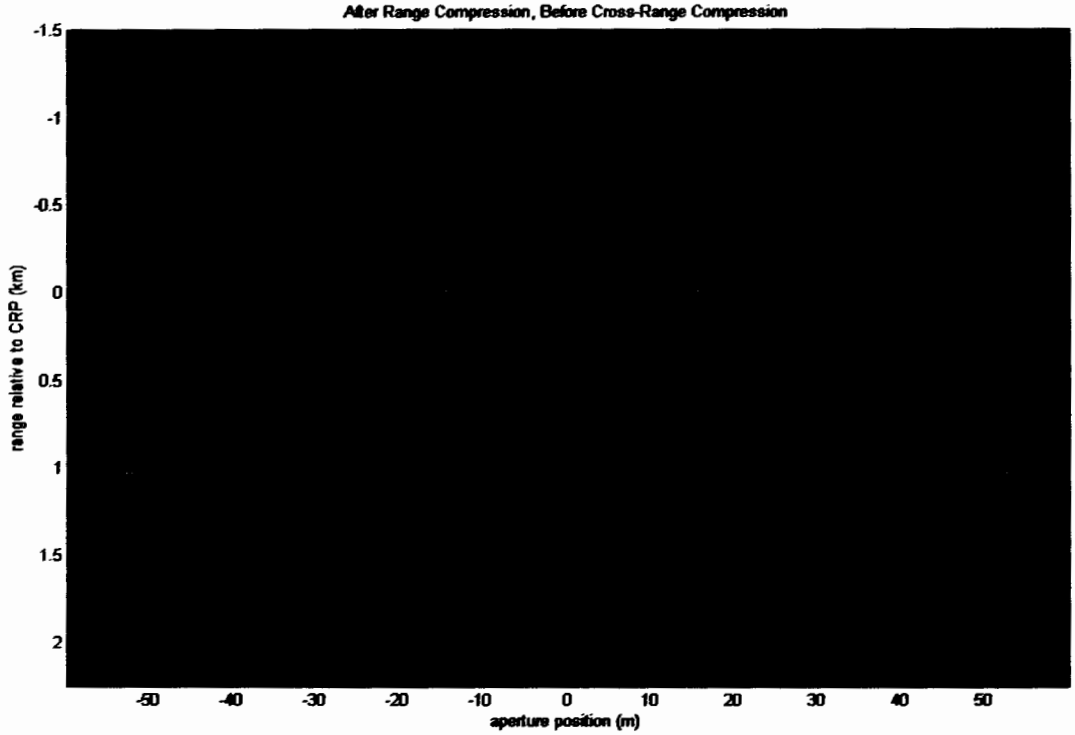

Figure 7.20: After applying Pulse compression to Dataset

7.4.3 Axis Mapped Image (Range & Cross-range)

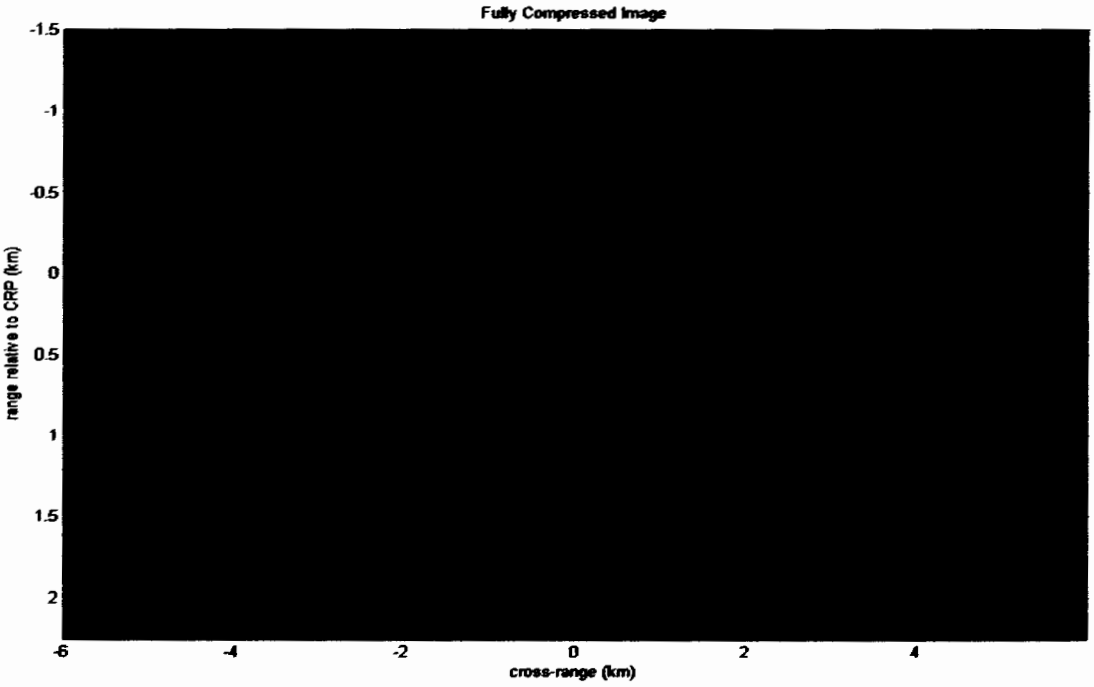

Figure 7.21: Final image after azimuth compression

CHAPTER 8 CONCLUSION AND FUTURE WORK

In the current research endeavor different SAR design parameters of airborne and spaceborne sensors are studied and critically analyzed. This research work is recommended to initiate research in the field of SAR. This dissertation provides a feasibility report on SAR sensors design parameters. Suitable designing parameters are selected and were simulated in this dissertation.

We conclude that for low-cost SAR design X-band is most suitable band due to it's easily and economically availability of components. To improve the resolution it would be desirable to reduce the effective beamwidth which can be achieved by its inverse relationship with antenna aperture. Synthesizing large aperture will produce a narrow beamwidth. Range-Doppler coupling property of LFM pulse reduces computational complexities and helps in finding true range resolution.

In future development we can use Range Doppler algorithm (RDA) in the signal processing part of the system. RDA is another algorithm for processing continuously collected SAR data into an image. It is computationally efficient and, for typical spaceborne imaging geometries, the range-Doppler algorithm is an accurate approximation to the exact SAR transfer function.

Another improvement in this project can be brought by using Spotlight mode and Interferometric synthetic aperture radar mode for determining accurate position of the terrain and comparing their results.

REFERENCES

[1] M. Usman "An imaging system utilizing Reflected GPS signals and Based on SAR Techniques" PhD dissertation 2009, University of Manchester UK.

[2] Y. K. Chan and V. C. Koo, "An introduction to Synthetic aperture radar (SAR)", Progress in Electromagnetics Research B, **2**, 27-60, 2008.

[3] See e.g.; http://www.sandia.gov/RADAR/sar.html.

[4] See e.g.; Cumming, Ian G and Wong, Frank H, "Digital Processing of Synthetic Aperture Radar Data: Algorithms and Implementations", Page: 113-151, Norwood, MA: Artech House, Inc., 2005.

[5] Glossary of remote sensing terms. Natural Resources Canada. [Online] Canada Center of Remote Sensing, November 21, 2005, See e.g; http://www.ccrs.nrcan.gc.ca/glossary/index_e.php?id=2284.

[6] See e.g.; Soumekh, Mehrad, "Synthetic Aperture Radar Signal Processing with MATLAB Algorithms", New York, NY: Wiley & Sons, Inc., 1999.

[7] Samuel W., McCandless, Jr. et al, "Chapter 1.Principles of Synthetic Aperture Radar", User system enterprises & Radar Imaging resources, Alexandria, VA USA.

[8] Lame, D.B., and G.H. Born, 1982, "SEASAT measurement system evaluation: Achievement and limitations", J.Geophys Res., 87 (C5), 3175-3178.

[9] Elachi, C., J Cimino, and M.Settle, 1986, "Overview of the Shuttle Imaging Radar-B preliminary scientific results", Science, **232**, 1511-1516.

[10] Way, J., and E. A. Smith, 1991, "The evolution of synthetic aperture radar systems and their progression to the EOS SAR", IEEE Trans. Geosci. Remote Sens., **29**, 962-985.

[11] Li, F.L., and R. K. Raney, 1991, "Prolog to special section on spaceborne radars of earth and planetary observations", Proc. IEEE, **79**, 773-776.

[12] ESA, 1991: ERS-1 special issue. ESA Bulletin, 65. [Available from the ESA publications Division, 8-10 rue-Mario-Nikis, 75738 Paris Cedex 15].

[13] Nemoto, Y., H. Nishino, M. Ono, H. Mizutamari, K. Nishikawa, and K. Tanaka, 1991, "Japanese Earth Resources Satellite-1 Synthetic aperture Radar", Proc. IEEE, **79**, 800-809.

[14] Evans, D. L., Ed., 1995, "Spaceborne Synthetic Aperture Radar: Current status and future directions", NASA Tech. Memo. 4679, Page.171.

[15] Jorden, R. L., B. L. Huneycutt, and M. Werner, 1991, "The SIR-C/X-SAR Synthetic Aperture Radar System", Proc. IEEE, **79**, 827-838.

[16] Zebker, H. A. and J.J Van Zyle, 1991, "Imaging radar polarimetry: A review", Proc. IEEE, **79**, 1583-1606.

[17] Rosen, P. A., S. Hensley, I. R Joughin, F. K. Li, S.N. Madsen, E. Rodriguez, and R. M. Goldstein, 2000, "Synthetic aperture radar interferometry", Proc. IEEE, **88**, 333-382.

[18] S.I Tsundo, F.Pace, J.Stence, W.H Hensely, A. W. Doerry and B. C. Walker, Lynx, A high-resolution synthetic aperture radar", SPIE Aerosense 1999, **3704**.

[19] P. Steeghs, E. V. Halsema and Peter Hoogeboom, "MINISAR: A miniature, lightweight, low cost scalable SAR system", TNO Physics and Electronics Laboratory and Delft University of Technology, IRCTR, Delft, The Netherlands. CEOS-SAR01-034.

[20] See e.g.; Http:// www.selex-sas.com.

[21] Evan C. Zaugg, Derek L. Hudson and David G. Long, "The BYU μSAR: A Small, Student-Built SAR for UAV operation", Microwave Earth Remote Sensing Laboratory Brigham Young University.

[22] See e.g.; RF, RFIC & Microwave Theory Design, www.rfic.co.uk pp 1-18.

[23] See e.g.; Donald R. Wehner, "High-Resolution Radar", 2nd Edition Artech House 1994.

[24] International Telecommunication Union's (ITU) World Radiocommunication Conference 1997 (WRC-97).

[25] Birk, R., W. Camus, E. Valenti, and W. J. McCandles, "Synthetic aperture radar imaging system," IEEE Aerospace and Electronic System Magazine, **10**, No. 11, 15-23, 1995.

[26] See e.g.; Skolink, M. I., "Radar handbook", McGraw-Hill, New York, 1970.

[27] See e.g.; Ulaby, F. T., R. K. Moore, and A. K. Fung, "Microwave remote Sensing: Active and passive", I, Artech House, Norwood, 1981.

[28] Hyyppa, J., J. Pullianinen, K. Heiska, and M. T. Hallikainen, "Statistics of backscattering source distribution of boreal coniferous forests at C- and X-band", Proceeding of the 1986 International Geosciences and Remote Sensing Symposium, **1**, 241-242, 1986.

[29] Pullianinen, J. T., K. Heiska, J. Hyyppa, and M. T. Hallikanien, "Backscattering properties of boreal forests at the C- and X-bands," IEEE Trans on Geosc. And remote sensing, **32**, No. 5, 1041-1050, 1994.

[30] See e.g.; Http://envisat.esa.int/handbooks/asar/CNTR2-.htm#eph.asar.prodalg. levb.alg. physjust.radgeo.

[31] See e.g.; Http://envisat.esa.int/handbooks/asar/CNTR5-2.htm.

[32] Juha Karvonen, "Compaction of C-band Synthetic Aperture Radar Based Sea Ice Information for navigation in the Baltic sea", PhD dissertation, Helsinki University of Technology, Finland. December 2006.

[33] H. Ottl, "The Real Aperture antenna of SAR, A key element for performance", Institute fur Hochfrequenztechnik, Germany.

[34] Anthony Freeman, "on ambiguities in SAR design", Jet Propulsion Laboratory, USA.

[35] Samuel W. McCandless1, Christopher R.Jackson2, "Principles of Synthetic Aperture Radar". 1. User systems enterprises, Inc., Denver, Co, USA. 2. Radar imaging resources, Alexandria, VA USA.

[36] Ajmal Ismail Mohungoo, "An airborne X-band Synthetic Aperture Radar receiver design and implementation" Master thesis, University of Cape Town, January 2004.

[37] See e.g.; D. R. Wehner, "High Resolution Radar", Artech House, Norwood, MA, 2nd edition, 1995.

[38] See e.g.; J. Curlander and R. McDonough, "Synthetic Aperture Radar: Systems and Signal Processing", John Wiley & Sons, New York, 1991.

[39] R. K. Raney, "Radar Fundamentals: Technical Prespective. In Manual of Remote Sensing", **2**: Principles and Applications of Imaging Radar, F. M. Henderson and A. J. Lewis (ed.), pp. 9-130. John Wiley & Sons, New York, 3rd edition, 1998.

[40] See e.g.; Http:// en.wikipedia.org/wiki/History_of_radar.

[41] See e.g.; Http://linkinghub.elsevier.com/retrieve/pii/S1874608X98800058.

[42] See e.g.; Http://pqasb.pqarchiver.com/washingtonpost/access/72199507.html.

[43] See e.g.; Http://www.solarviews.com/cap/venus/alpha1.htm.

[44] David E. Weissman, David B. King and, and Thomas W. Thompson, "Relationship between Hurricane Surface Winds and L-Band Radar Backscatter from the Sea Surface", Jet Propulsion Laboratory, Pasadena, CA 91103, August 1979.

[45] See e.g.; Http:// docs.lib.purdue.edu/lars_symp/316.

[46] Paris W. Vachon, Richard B. Olsen, Harald E. Krogstad and Antony K. Liu, "Airborne Synthetic Aperture Radar Observations and Simulations for Waves in Ice". Journal of geophysical research, **98**, No. C9, PP. 16,411-16,425, 1993.

[47] See e.g.; Http://www.jpl.nasa.gov/news/releases/80s/release_1987_1173.html.

[48] See e.g.; Http://www.fas.org/spp/military/docops/army/ref_text/chap07e.htm.

[49] See e.g.; Http://www.nasaimages.org/luna/servlet/detail/NVA2~14~14~27939 ~124435:L-&-C-bands-Canberra,-Australia?printerFriendly=1.

[50] Wolfgang Keydel, "Present and Future Airborne and Space-borne Systems", Microwaves and Radar Institute German Aerospace Research Center (DLR). Germany.

[51] R. Horn: "The DLR Airborne SAR Project E-SAR", Proceedings of IGARSS'96 Lincoln, Nebraska USA. Pp. 1624-1626, 1996.

[52] R. Scheiber, A. Ulbricht, A. Reigber, K.P Papathanassiou, "Airborne Interferometric SAR activities in DLR", RTO Meeting, High Resolution Radar Techniques. Granada, Spain March 1999.

[53] A. Potsis, N. Uzunglou, P. Frangos, R. Horn, K. Lamprecht, "Analysis of P-band Synthetic Aperture Radar for Airborne and Spaceborne Applications", RTO meeting, Space-based Observation Technology. Island of Samos, Greece. 16-18 october 2000.

[54] Edrich, M. Weiss, G. "Second-generation Ka-Band UAV SAR system".

[55] Remy Chapoulie, Michel Matinaud, Philippe Paillo, Dany Barrand, Philippe Dreuillet, "The Airborne Ramses radar experiment for archaeological prospecting in a temperate climate region", ONERA, 91761 Palaiseau cedex, France.

[56] P. Snoeij, P. Hoogeboom, P. Koomen and H. Pouwels, "The PHARUS airborne polarimetric C-Band SAR Project", Physics and Electronics Laboratory (TNO-FEL), National Aerospace Laboratory NLR and the Delft University o Technology, Telecommunication and remote sensing Laboratory Netherland.

[57] Philippe Steeghs, Erick Van Halsema and Peter Hoogeboom, "Mini-SAR: A miniature, lightweight, low cost, scalable system", TNO Physics and Electronics Laboratory and Delft University of Technology, IRCTR, Delft, The Netherlands.

[58] Evan C. Zaugg, Derek L. Hudson and David G. Long, "The BYU μSAR: A Small, Student-Built SAR for UAV operation", Microwave Earth Remote Sensing Laboratory Brigham Young University.

[59] M.I Duersch, "BYU Micro-SAR: A very Small, Low power, LFM-CW Synthetic Aperture Radar," Master's Thesis, Brigham Young University, Provo, Utah, 2004.

[60] J. T. Sri sumantyo, H. Wakabayashi et al,. "Development of Circularly Polarized Synthetic Aperture Radar Onboard Microsatellite (μ SAT CP-SAR)", PIERS Proceedings, Beijing, China, March 23-27, 2009.

[61] See e.g.; E D Kaplan "Understanding GPS Principles and application", Artech House Publishers

[62] See e.g.; Bernard Sklar "Digital Communication fundamentals and application", Prentice Hall International edition.

[63] Dr Gott Class Notes "Digital Communication", MSc Communication Engineering UMIST 2003.

[64] See e.g.; Peyton Z. Peebles, Jr "Radar Principles", John Wiley & Sons, Inc.

[65] See e.g.; Http://www.wikipedia.com

[66] See e.g.; Mark A. Richards "Fundamentals of Radar Signal Processing", Artech House Publishers